# A comparative study on the control of friction-driven oscillations by time-delayed feedback

**ARTICLE** *in* NONLINEAR DYNAMICS · APRIL 2010

Impact Factor: 2.85 · DOI: 10.1007/s11071-009-9577-x



**3 AUTHORS:**

Ashesh Saha
Indian Institute of Technology Kanpur
**7** PUBLICATIONS **25** CITATIONS
SEE PROFILE

Bishakh Bhattacharya
Indian Institute of Technology Kanpur
**62** PUBLICATIONS **150** CITATIONS
SEE PROFILE

Pankaj Wahi
Indian Institute of Technology Kanpur
**54** PUBLICATIONS **284** CITATIONS
SEE PROFILE

Nonlinear Dyn (2010) 60: 15–37
DOI 10.1007/s11071-009-9577-x

ORIGINAL PAPER

# A comparative study on the control of friction-driven oscillations by time-delayed feedback

**Ashesh Saha · Bishakh Bhattacharya · Pankaj Wahi**

Received: 4 May 2009 / Accepted: 4 August 2009 / Published online: 27 August 2009


**Abstract** We perform a detailed study of two linear time-delayed feedback laws for control of friction-driven oscillations. Our comparative study also includes two different mathematical models for the nonlinear dependence of frictional forces on sliding speed. Linear analysis gives stability boundaries in the plane of control parameters. The equilibrium loses stability via a Hopf bifurcation. Dynamics near the bifurcation is studied using the method of multiple scales (MMS). The bifurcation is supercritical for one frictional force model and subcritical for the other, pointing to complications in the true nature of the bifurcation for friction-driven oscillations. The MMS results match very well with numerical solutions. Our analysis suggests that one form of the control force outperforms the other by many reasonable measures of control effectiveness.

**Keywords** Friction-induced vibration · Hopf bifurcation · Time-delayed feedback control

## 1 Introduction

In this paper, we use linear time-delayed position feedback for the control of friction-driven vibrations. We have considered a single-degree-of-freedom (SDOF) spring–mass–damper on a moving belt as our physical system. Two different forms of these control forces popular in the literature have been considered and a comparative study is performed on the effectiveness of these forces in quenching these vibrations. Two different mathematical models for dry friction, which differ qualitatively in the dynamic behavior, have also been considered highlighting the need for a detailed experimental study to unravel the true dynamic behavior of friction-induced vibrations.

Friction-induced vibrations, a type of self-excited oscillation (refer to [1, 2]), are a frequently encountered problem in many engineering systems (e.g., brake-squeal, train curve squeal, clutch chatter, machine-tool chatter, vibrations in controlled positioning systems). The drooping characteristic of the friction force (decrease in the friction force with an increase in the relative velocity) in the low relative velocity regime has been established as one of the major causes of such violent vibrations [2]. With an increase in the relative velocity past some critical value, the friction force either increases with an increase in the relative velocity or attains a constant value. As a result, the system undergoes bounded periodic motions, the so-called limit cycle oscillations. Since these self-excited vibrations are highly undesirable in most engineering applications, it is useful to get a better understanding of the phenomena to develop efficient methods for controlling such oscillations.

Several friction models have been proposed in the literature for modeling frictional slip [3–12]. These

A. Saha · B. Bhattacharya · P. Wahi (✉)
Mechanical Engineering Department, Indian Institute of Technology, Kanpur, 208016, India
e-mail: wahi@iitk.ac.in

models incorporate varying physical phenomena associated with friction. The most popular models among researchers focusing on friction-induced vibrations include the exponential friction model proposed by Hinrichs et al. [3] and a polynomial type friction model proposed by Thomsen [4] (motivated by a model given in the book by Panovko and Gubanova [5]). These simple empirical models account only for the drooping characteristics of the friction force and do not take into account other aspects, like hysteresis and acceleration. However, the force during frictional slip is known to be complicated and depends on several other parameters [6]. As early as in 1983, Ruina [6] discussed some experimentally motivated internal state variable friction laws which may depend on slip rate and/or slip distance for modeling friction under unsteady conditions. The effect of these on stability of steady sliding was also considered therein. In recent times, McMillan [7] considered a phenomenological model wherein the friction force depends on the acceleration and as a result there is hysteresis near zero relative velocity. Some other recent models of friction incorporate the microscopic degrees of freedom, and such models are known as dynamic models of friction [8–12]. The LuGre model proposed by Canudas de Wit et al. [8] is the most widely used form of the microscopic model of friction. In this model, the asperities of the friction interface are considered as elastic spring-like bristles and this model accounts for several of the known physical phenomena related to friction. More realistic friction models qualitatively showing a larger variety of observed frictional behavior have been obtained by appropriate modifications of the LuGre model; e.g. the elasto-plastic friction model [9], the Leuven model [10, 11] and the generalized Maxwell-slip friction model [12]. Awrejcewicz and Olejnik [13] reviewed most of the friction models and the related system dynamics. In this paper, we have considered the exponential friction model [3] as well as the polynomial friction model (as used by Thomsen [4]). These two models account for the same physical phenomenon, viz. instability due to the drooping characteristic of the friction force, but differ in their qualitative dynamic behavior. This happens because stability of the system is governed by the slope of the control force vs. relative velocity plot at the operating point which is negative for both the models while the nonlinear behavior is dictated by higher-order derivatives, and these models differ in the sign of the third derivative of the control force w.r.t. the relative velocity. Detailed experimental study is, therefore, required to ascertain the true qualitative dynamic behavior of these vibrations and understanding the role of the various process parameters in determining them. This will be carried out in our future work.

Most studies on friction-induced vibrations either consider a rigid mass on a moving belt system or they model their physical system using this idealization. Awrejcewicz and Olejnik [13, 14] analyzed the nonlinear phenomena exhibited by a duo-servo brake system with dry friction. They modeled the brake mechanism by a two-degrees-of-freedom mass on a moving belt system where the normal load varies with the displacement of the mass. The response of a SDOF dry friction oscillator under (a) constant belt velocity, (b) harmonic driving force, and (c) their combination is investigated by Andreaus and Casini [15]. The dynamical behavior of a dry friction oscillator with simultaneous self- and external excitation is analyzed by Hinrichs et al. [3]. Hetzler et al. [16] studied the stability and local bifurcation behavior of the exponential friction model [3] in the pure sliding domain of a SDOF friction oscillator. Li and Feng [17] performed a preliminary bifurcation study of a SDOF oscillator with the LuGre friction model and observed chaotic motions, stick-slip motions and period doubling phenomenon.

Several strategies have been investigated in recent times for controlling friction-induced vibrations. High frequency tangential excitation was proposed by Thomsen [4] for controlling these self-excited oscillations, and its effectiveness in controlling stick-slip chaos in a frictional oscillator was experimentally studied by Feeny and Moon [18]. Popp and Rudolph [19] discussed fluctuating normal load due to a geometrically nonlinear coupling of modes as a passive means to control friction-induced stick-slip motion. Chatterjee [20] analyzed an externally imposed normal-force modulation as a means to control these vibrations. Heckl and Abrahams [21] proposed an active control scheme based on a phase-shifted velocity feedback for quenching friction-induced oscillations. Active control of a floating caliper disc brake squeal using ‘smart pads’ composed of piezoceramic staple actuators and optimal feedback control strategy has been experimentally investigated by von Wagner et al. [22].

Time-delayed control has become very popular among researchers focusing on feedback control.

Atay [23] and Maccari [24, 25] investigated the use of time-delayed state feedback method in controlling free, forced and parametric vibrations in the van der Pol oscillator. Hu et al. [26] studied the primary resonance and 1/3 subharmonic resonance of a harmonically forced Duffing oscillator under state feedback with a time delay. The effectiveness of delayed position feedback in controlling payload pendulations in rotary cranes was demonstrated by Masoud et al. [27], while Jnifene [28] considered control of vibrations in a single-link flexible manipulator. Qian and Tang [29] considered time-delayed feedback controller for the instability of a nonlinear beam under moving load. However, there are very limited studies concentrating on its use for control of friction-induced vibrations. Das and Mallik [30] considered time-delayed PD feedback control of self-excited and forced vibrations of a friction-driven system. Chatterjee [31] has investigated time-delayed feedback control of different types of friction-induced instabilities. Neubauer et al. [32] presented the use of time-delayed position feedback to control stick-slip vibrations and experimentally investigated time-delayed velocity feedback for control of an automotive disc brake. Although the control forces in [30] and [31] are differing in functional form, they are applied in the same direction which is parallel to the friction force. However, the control force in [32] is applied in the normal direction. In our analysis, we will consider the control forces as in [30] and [31] and compare their effectiveness in quenching these oscillations.

The rest of the paper is organized as follows. In Sect. 2, we present our mathematical model with the two different friction models and the two control forces derived from time-delayed position feedback. Section 3 analyzes the system with the polynomial friction model. Linear stability analysis and nonlinear analysis by two different approaches have been performed. Similar analysis for the friction oscillator with the exponential friction model is briefly presented in Sect. 4. In Sect. 5, we compare the efficacy of the control forces in quenching friction-driven oscillation using different measures of control performance. Finally, some conclusions are drawn in Sect. 6.

## 2 The mathematical model

We consider a simplified model for the study of friction-induced vibrations consisting of a spring–mass–damper system with the mass resting on a friction belt moving with a constant velocity as shown in Fig. 1.

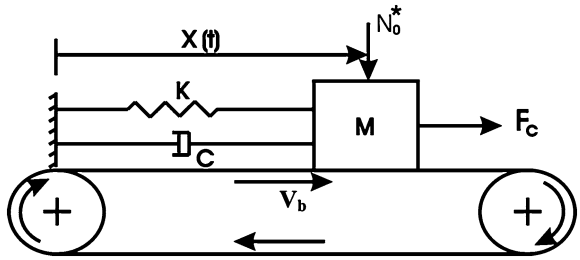


**Fig. 1** Damped harmonic oscillator on a moving belt as a model for friction-driven vibrations

The equation of motion of the system is given as

$$M\frac{d^2X}{dt^2} + C\frac{dX}{dt} + KX = F(V_r) + F_c, \tag{1}$$

where $F(V_r) = N_0^*\mu(V_r)$ is the friction force ($N_0^*$ is the total normal load including the weight of the slider and $\mu(V_r)$ is the friction function) and $F_c$ is the control force. Note that we have assumed a linear dependence of the friction force on the normal load. In reality this dependence could be nonlinear as well. However, this does not affect the analysis in the current paper since the normal load is assumed to be a constant. We will consider two different control forces (as in [31] and [30]), viz.

$$(F_c)_1 = -K_{c1}^*\big(X - X(t - T_1^*)\big), \tag{2a}$$

$$(F_c)_2 = K_{c2}^* X(t - T_2^*) \tag{2b}$$

for the analysis in this paper. $K_{c1}^*$, $K_{c2}^*$ are the control gains and $T_1^* > 0$, $T_2^* > 0$ are the time delays. There is no a priori assumption on the sign of the control gains, and hence, the direction of the control force in Fig. 1 is not critical. In all future discussions, we will focus only on the case $K_{c1}^* > 0$, $K_{c2}^* > 0$ and any required change in the sign of the control forces would be achieved by suitably adjusting the time delays.

The non-dimensionalized form of the equations of motion (using the characteristic time scale fixed by $\omega_0 = \sqrt{K/M}$ and the characteristic length by $x_0 = N_0^*/(M\omega_0^2)$) with the control forces 1 and 2 is

$$x'' + 2\xi x' + x = \mu(v_r) - K_{c1}\big(x - x(\tau - T_1)\big), \tag{3a}$$

$$x'' + 2\xi x' + x = \mu(v_r) + K_{c2}x(\tau - T_2), \tag{3b}$$

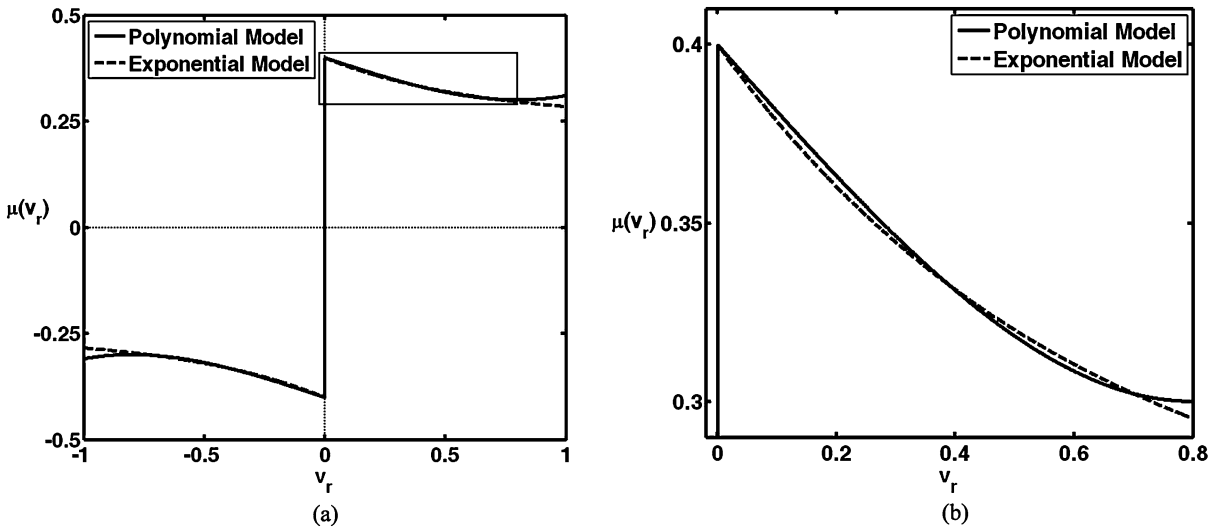


**Fig. 2** (**a**) The friction force versus the relative velocity for the two friction models; (**b**) A zoomed view of the boxed region in (**a**). Parameters: $\mu_s = 0.4$, $\mu_m = 0.3$, $v_m = 0.8$, $\mu_k = 0.255$, $a = 1.6$

where primes denote derivative with respect to the non-dimensional time $\tau = \omega_0 t$. The other non-dimensional quantities are:

$$T_1 = \omega_0 T_1^*, \qquad T_2 = \omega_0 T_2^*, \qquad \xi = \frac{C}{2M\omega_0},$$

$$x = \frac{X}{x_0}, \qquad v_b = \frac{V_b}{\omega_0 x_0}, \qquad K_{c1} = \frac{K_{c1}^*}{M\omega_0^2},$$

$$K_{c2} = \frac{K_{c2}^*}{M\omega_0^2}, \qquad v_r = \frac{V_r}{\omega_0 x_0} = \frac{V_b - \dot{X}}{\omega_0 x_0} = v_b - x'.$$

We will also consider two different functional forms for the friction force. The first one is a polynomial type representation (as used by Thomsen [4])

$$\mu(v_r) = \mu_s \mathrm{sgn}(v_r) - \frac{3}{2}(\mu_s - \mu_m)\left(\frac{v_r}{v_m} - \frac{1}{3}\left(\frac{v_r}{v_m}\right)^3\right), \tag{4}$$

where $v_r = v_b - x'$ is the (non-dimensional) relative velocity between the mass and the belt, $\mu_s$ is the coefficient of static friction, and $v_m$ is the velocity corresponding to the minimum coefficient $\mu_m$ of kinetic friction, $\mu_m \leq \mu_s$. We will also use the exponential friction model [3] given by

$$\mu(v_r) = \left(\mu_k + \Delta\mu e^{-a|v_r|}\right)\mathrm{sgn}\,(v_r), \tag{5}$$

where $\Delta\mu = \mu_s - \mu_k$, $\mu_s$ is the coefficient of static friction, $\mu_k$is the minimum coefficient of kinetic friction, and $a$ is the slope parameter. Both the friction models with some typical parameter values are shown in Fig. 2. For this particular choice of parameter values, the two curves match reasonably well up to an absolute relative velocity of 0.8. This regime of relative velocity along with this particular set of parameters, i.e., $\mu_s = 0.4$, $\mu_m = 0.3$, $v_m = 0.8$, $\mu_k = 0.255$, and $a = 1.6$, will be used for comparing the two friction models. A set of experimentally obtained data points in this range can be fitted to any one of these two friction models. The two friction models have negative slope (for any relative velocity in the interval of interest 0–0.8) which governs the stability of the system. However, they differ in the sign of the rate of change of curvature, i.e., the third derivative of the force w.r.t. the relative velocity, and as a consequence, exhibit significantly different qualitative nature of the dynamic response. This observation is important as it warns against curve fitting of the experimental data points with any chosen function without invoking the physics behind the phenomenon. We restrict attention to the interval $v_r = 0$–$0.8$ resulting in a smooth function for the friction force and allowing us to use series expansions to get a polynomial representation required for the perturbation analysis. This assumption negates the possibility of stick-slip motion thereby effectively restricting motions to pure slipping.

Now consider the equation of motion (3a). The steady-state ($x'' = x' = 0$) solution is $x_{eq} = \mu(v_b)$. Similarly, the steady-state solution for the equation of motion (3b) is $x_{eq} = \frac{\mu(v_b)}{1-K_{c2}}$ (for $K_{c2} \neq 1$). Shifting the origin to the equilibrium solution by introducing the coordinate transformation $z = x - x_{eq}$ (i.e. $z' = x'$, $z'' = x''$) and after some straightforward manipulations, the equations of motion (3a) and (3b) for the polynomial friction model reduce to

$$z'' + z = h_1 z' + h_2 z'^2 + h_3 z'^3 - K_{c1}\big(z - z(\tau - T_1)\big), \quad \text{and} \tag{6a}$$

$$z'' + z = h_1 z' + h_2 z'^2 + h_3 z'^3 + K_{c2} z(\tau - T_2), \tag{6b}$$

where

$$h_1 = -2\xi + \alpha_1\left(1 - \left(\frac{v_b}{v_m}\right)^2\right), \qquad h_2 = \frac{\alpha_1}{v_m^2} v_b,$$
$$h_3 = -\left(\frac{\mu_s - \mu_m}{2v_m^3}\right) \quad \text{and} \tag{7}$$
$$\alpha_1 = \frac{3}{2}\left(\frac{\mu_s - \mu_m}{v_m}\right) > 0.$$

The non-dimensionalized equations of motion for the two control forces in the transformed coordinates are

$$z'' + z = -2\xi z' + \gamma\left(e^{az'} - 1\right) - K_{c1}\big(z - z(\tau - T_1)\big), \quad \text{and} \tag{8a}$$

$$z'' + z = -2\xi z' + \gamma\left(e^{az'} - 1\right) + K_{c2} z(\tau - T_2) \tag{8b}$$

for the exponential friction model, where $\gamma = \Delta\mu e^{-av_b}$.

## 3 Analysis of the system with the polynomial friction model

### 3.1 Linear stability analysis

We first linearize (6a) and (6b) about the equilibrium ($z = 0$) to get

$$z'' + (1 + K_{c1})z - h_1 z' = K_{c1} z(\tau - T_1), \quad \text{and} \tag{9a}$$

$$z'' + z - h_1 z' = K_{c2} z(\tau - T_2). \tag{9b}$$

The corresponding characteristic equations are

$$s^2 - h_1 s + (1 + K_{c1}) - K_{c1} e^{-sT_1} = 0, \quad \text{and} \tag{10a}$$

$$s^2 - h_1 s + 1 - K_{c2} e^{-sT_2} = 0. \tag{10b}$$

On the stability boundary, either the most dominant pair of roots becomes purely imaginary, i.e., $s = \pm j\omega$ (a Hopf bifurcation), or the most dominant root is at the origin, i.e., $s = 0$. Typically a root at the origin is associated with bifurcations to other steady-state solutions. However, the form of nonlinearity associated with our model precludes any other steady state and, hence, the solutions diverge after loss of stability past $s = 0$.

We first investigate the stability boundary corresponding to the Hopf bifurcation and, therefore, we substitute $s = j\omega$ into (10a) and (10b), where $\omega$ determines the frequency of the ensuing periodic solution. Separating the real and imaginary parts of the equations, gives us

$$\omega^2 - (1 + K_{c1}) + K_{c1}\cos(\omega T_1) = 0, \tag{11a}$$

$$h_1\omega = K_{c1}\sin(\omega T_1) \tag{11b}$$

for (10a) and

$$\omega^2 - 1 + K_{c2}\cos(\omega T_2) = 0, \tag{12a}$$

$$h_1\omega = K_{c2}\sin(\omega T_2) \tag{12b}$$

for (10b). These can be solved for the two unknowns ($K_{c1,c2}$ and $T_{1,2}$) with the other unknown $\omega$ as the parameter for a given $v_b$. The parametric dependence of the critical values of $K_{c1,c2}$ and $T_{1,2}$ on $\omega$ for (10a) and (10b) is given by

$$K_{c1o} = \frac{(\omega^2 - 1)^2 + h_1^2\omega^2}{2(\omega^2 - 1)},$$
$$T_{1o} = \frac{2}{\omega}\left[\tan^{-1}\left(\frac{\omega^2 - 1}{h_1\omega}\right) + 2i\pi\right] \tag{13a}$$
$$\forall i = 0, 1, 2, \ldots, \infty,$$

$$K_{c2o} = \sqrt{(1 - \omega^2)^2 + h_1^2\omega^2},$$
$$T_{2o} = \frac{1}{\omega}\left[\tan^{-1}\left(\frac{h_1\omega}{1 - \omega^2}\right) + 2i\pi\right] \tag{13b}$$
$$\forall i = 0, 1, 2, \ldots, \infty.$$

For a Hopf bifurcation to occur, the characteristic roots must cross the imaginary axis transversally. Therefore, the sign of the following quantities (considering the control gains as the bifurcation parameter)

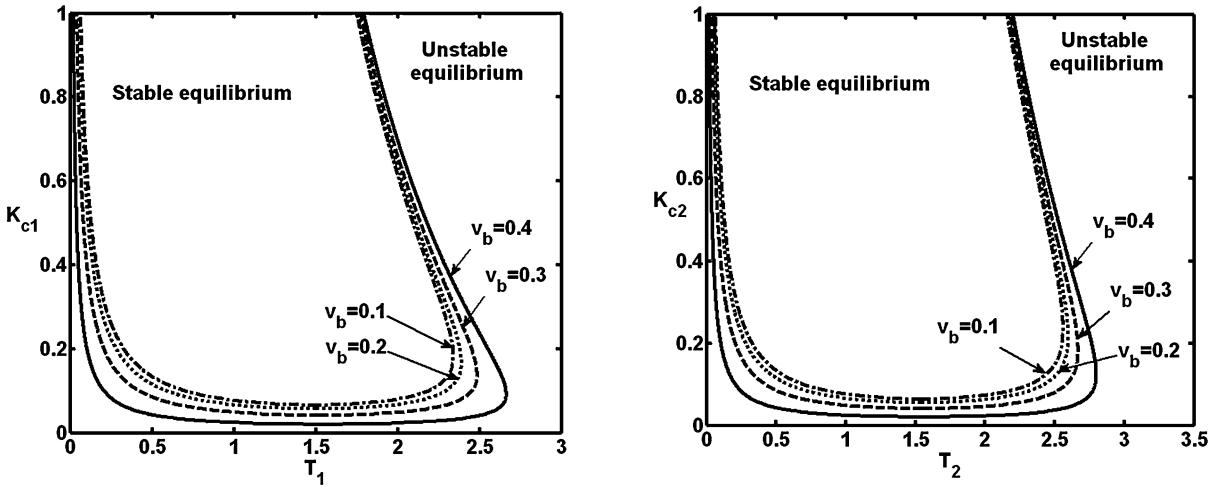


**Fig. 3** Stability boundaries for (**a**) control force 1 and (**b**) control force 2. Parameters: $\xi = 0.06$, $\mu_s = 0.4$, $\mu_m = 0.3$, $v_m = 0.8$

must also be checked:

$$\begin{aligned} &R_1(\omega_c, K_{c1o}) \\ &= \text{sgn}\left[\text{Re}\left(\frac{ds}{dK_{c1}}\bigg|_{j\omega_c, K_{c1o}}\right)\right] \\ &= \text{sgn}\left[(h_1 + K_{c1o}T_{1o})\big(1 - \cos(\omega_c T_{1o})\big)\right. \\ &\quad \left. - 2\omega_c \sin(\omega_c T_{1o})\right], \end{aligned} \tag{14a}$$

$$\begin{aligned} &R_2(\omega_c, K_{c2o}) \\ &= \text{sgn}\left[\text{Re}\left(\frac{ds}{dK_{c2}}|_{j\omega_c, K_{c2o}}\right)\right] \\ &= \text{sgn}\left[K_{c2o}T_{2o} - h_1 \cos(\omega_c T_{2o})\right. \\ &\quad \left. - 2\omega_c \sin(\omega_c T_{2o})\right]. \end{aligned} \tag{14b}$$

If $R_{1,2} < 0$, the equilibrium becomes stable for $K_{c1,c2} > K_{c1o,c2o}$ and if $R_{1,2} > 0$, the equilibrium becomes unstable for $K_{c1,c2} > K_{c1o,c2o}$. The stability boundary corresponding to the Hopf bifurcation in the plane of control parameters ($K_{c1}$ vs. $T_1$) for control force 1 is plotted using (13a) in Fig. 3(a) and the stable region is identified using (14a). A similar diagram is presented for control force 2 using (13b) and (14b) in Fig. 3(b).

To complete the stability diagram, we need to consider the case $s = 0$. This case is obtained by replacing $\omega = 0$ in (11) and (12). Substitution of $\omega = 0$ into (11a) leads to the contradiction $1 = 0$ and, hence, this scenario cannot happen for control force 1 and therefore there is no restriction on $K_{c1}$. A similar substitution into (12a) gives us $K_{c2} = 1$ and we can easily verify that $R_2 > 0$. Therefore, the solutions will diverge for control force 2 when $K_{c2} > 1$. Hence, the stability regime for control force 2 is bounded above by $K_{c2} = 1$. This restriction is, however, not severe as we can achieve stability for significantly smaller values of $K_{c2}$.

As mentioned above, Fig. 3 shows the stability boundaries separating the stable and unstable regions of the static equilibrium for different belt velocities. The belt velocities are chosen to be less than the critical belt velocity corresponding to the Hopf bifurcation point of the uncontrolled system such that the static equilibrium of the uncontrolled system is unstable. The stability region increases with an increase in the belt velocity as expected. The stability boundary for the case of the critical belt velocity corresponding to the Hopf point of the uncontrolled system can be obtained analytically in closed form following the analysis in [35].

Using (7) and (11b) (for control force 1) and (7) and (12b) (for control force 2), we can get the critical belt velocities $(v_b)_{c1}$ and $(v_b)_{c2}$ corresponding to the Hopf bifurcation point for given values of the control gain and the time delay as

$$(v_b)_{c1} = v_m \sqrt{1 - \frac{1}{\alpha_1}(h_1 + 2\xi)}$$

$$= v_m\sqrt{1-\frac{1}{\alpha_1}\left(\frac{K_{c1}\sin(\omega_1 T_1)}{\omega_1}+2\xi\right)}, \quad (15a)$$

$$(v_b)_{c2} = v_m\sqrt{1-\frac{1}{\alpha_1}(h_1+2\xi)}$$

$$= v_m\sqrt{1-\frac{1}{\alpha_1}\left(\frac{K_{c2}\sin(\omega_2 T_2)}{\omega_2}+2\xi\right)}, \quad (15b)$$

where $\omega_1$ and $\omega_2$ are to be obtained from (11a) and (12a), respectively.

### 3.2 Nonlinear analysis

In this subsection, we perform a nonlinear stability analysis to ascertain the nature of the Hopf bifurcation. This subsection also highlights the difference between the results obtained using two different asymptotic methods, viz. averaging (as in [31, 33]) and the method of multiple scales (as in [34, 35]). Both the methods require the nonlinear terms to be small, but differ in the treatment of the linear damping and the delayed term. When using the averaging, we must treat damping and the delayed terms as small. For example, the equation for control force 2 has to be written as

$$z''+z=\varepsilon\big(h_1 z'+h_2 z'^2+h_3 z'^3+K_{c2}z(\tau-T_2)\big).$$

However, with the method of multiple scales (MMS), we can treat linear damping and the delayed terms as $\mathcal{O}(1)$, i.e., not small, thereby obtaining more accurate results. In particular, the equation for control force 2 would be

$$z''+z-h_1 z'-K_{c2}z(\tau-T_2)=\varepsilon h_2 z'^2+\varepsilon^2 h_3 z'^3.$$

Note that the MMS used in this paper is different from the one used in [30] wherein the delayed term and linear damping were treated as small thereby remaining closer in spirit to the method of averaging used in [31, 33].

#### *3.2.1 Averaging method*

As described above, to perform averaging, we rewrite (6a) and (6b) in the following form:

$$z''+z=\varepsilon f\big(z(\tau),z'(\tau),z(\tau-T_{1,2})\big), \quad 0<\varepsilon\ll 1, \quad (16)$$

where

$$\varepsilon f\big(z(\tau),z'(\tau),z(\tau-T_1)\big) = h_1 z'+h_2 z'^2+h_3 z'^3+K_{c1}z(\tau-T_1) - K_{c1}z(\tau) \quad \text{(for control force 1)}, \quad (17a)$$

and

$$\varepsilon f\big(z(\tau),z'(\tau),z(\tau-T_2)\big) = h_1 z'+h_2 z'^2+h_3 z'^3 + K_{c2}z(\tau-T_2) \quad \text{(for control force 2)}. \quad (17b)$$

The unperturbed system for $\varepsilon=0$ is a simple harmonic oscillator (SHO) and, hence, the system is effectively reduced to a perturbation of the SHO. The slowly varying solution of (16) is assumed (as in [31, 33]) to be

$$\begin{aligned} z &= A_1(\tau)\sin\big(\tau+\varphi_1(\tau)\big),\\ z' &= A_1(\tau)\cos\big(\tau+\varphi_1(\tau)\big). \end{aligned} \quad (18)$$

$A_1(\tau)$ and $\varphi_1(\tau)$ are slowly varying functions of time $\tau$. Hence, it is appropriate to assume $A_1(\tau-T)\approx A_1(\tau)$, and $\varphi_1(\tau-T)\approx\varphi_1(\tau)$ (see [33]). Thus, following the standard averaging method, we obtain

$$A_1'=\frac{1}{2}\big(h_1-K_c\sin(T)\big)A_1+\frac{3}{8}h_3 A_1^3, \quad (19)$$

where $h_1$ and $h_3$ are given by (7) and $K_c$ denotes $K_{c1}$ or $K_{c2}$ for the control forces 1 or 2, respectively. Similarly, $T$ denotes $T_1$ or $T_2$ for the control forces 1 or 2, respectively. The coefficient of the linear term contains the bifurcation parameter and changes sign at some critical value of the bifurcation parameter (the stability boundary) which is given by the zero level set of the function

$$L(T,K_c,v_b)=h_1-K_c\sin(T). \quad (20)$$

Figure 4 compares the stability boundary obtained using the averaging method with the exact stability boundary obtained using the linear stability analysis. It is observed that the stability boundaries obtained by the averaging method do not match the exact stability boundaries very well. The gross overestimation of the stability regimes by the averaging method is due to the approximation in (16) wherein $K_{c1}$ is $\mathcal{O}(\varepsilon)$ thereby restricting the analysis to small values of $K_{c1}$ only,

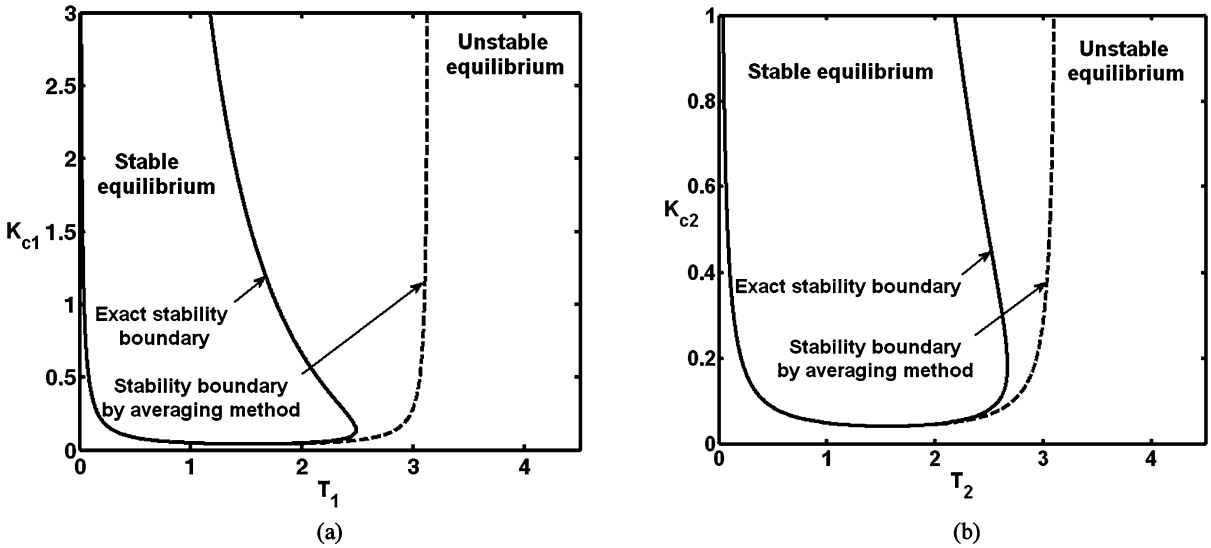


**Fig. 4** Comparison of the exact stability boundary with that obtained from the averaging method for the polynomial friction model. (**a**) Control force 1; (**b**) Control force 2. Parameters: $v_b = 0.3$, $\xi = 0.06$, $\mu_s = 0.4$, $\mu_k = 0.3$, $v_m = 0.8$

whereas the required values of $K_{c1}$ for stability are sufficiently large.

We observe from (19) that the linear term is negative in the stable region and becomes positive in the unstable region (e.g., if $K_c$ is considered a bifurcation parameter, we enter the unstable region for $K_c < K_{co}$ and therefore, $L(T, K_c, v_b) > 0$). Since $h_3 < 0$ (see (7)), we get a stable limit cycle in the linearly unstable regime signifying a supercritical Hopf bifurcation.

The approximate critical belt velocity (belt velocity corresponding to the Hopf bifurcation point) for a given control gain and time delay for the polynomial friction model with the two control forces is given by

$$(v_b)_{non} = v_m \sqrt{1 - \frac{1}{\alpha_1}\big(2\xi + K_c \sin(T)\big)}. \tag{21}$$

For operating belt velocities larger than this critical value, due to supercriticality of the Hopf bifurcation, the static equilibrium is globally stable. When the operating belt velocity is smaller than this value, the static equilibrium is unstable (based on the averaging results) and we get a stable limit cycle of amplitude (from (19))

$$A_1 = \sqrt{\frac{4}{3h_3}\big(K_c \sin(T) - h_1\big)}. \tag{22}$$

In what follows, we apply the method of multiple scales (MMS) [34, 35] wherein no assumption is made on the magnitude of the friction force or the control force, and the unperturbed equation corresponds exactly to the linearized delay differential equation (DDE) studied in Sect. 3.1. We will present our analysis using MMS for control force 2 only. The procedure for control force 1 follows exactly and is not presented here.

### 3.2.2 *Method of multiple scales (MMS)*

To cast (6b) in the standard form for applying the method of multiple scales, we require a small parameter, say $0 < \varepsilon \ll 1$, and we further require the nonlinear terms to be small. In order to achieve this goal, we transform coordinate as $z = \varepsilon y$ which after some straightforward manipulation leads to

$$y'' + y - h_1 y' - \varepsilon h_2 y'^2 - \varepsilon^2 h_3 y'^3 - K_{c2} y(\tau - T_2) = 0. \tag{23}$$

Next, we identify the Hopf point (i.e., the critical value of the bifurcation parameter $K_{c2o}$ at $T_2 = T_{2o}$ obtained from linear stability analysis, i.e., (13b)) and perturb it as follows: $K_{c2} = K_{c2o} + \varepsilon^2 \Delta$. Equation (23), then, becomes

$$y'' + y - h_1 y' - \varepsilon h_2 y'^2 - \varepsilon^2 h_3 y'^3$$

$$-\big(K_{c2o}+\varepsilon^2\Delta\big)y(\tau-T_{2o})=0. \tag{24}$$

For $\varepsilon=0$, (24) reduces exactly to the linearized equation (9b) whose solution is known to us.

We next define multiple time scales as: $t_0(\tau)=\tau$, the original time scale; and slow time scales $t_1(\tau)=\varepsilon\tau$, $t_2(\tau)=\varepsilon^2\tau$, and so on. Following [34, 35], the solution to (24) is assumed to be a function of these different independent time scales, as $y(\tau)=Y(t_0,t_1,t_2)$. Next, we expand $Y(t_0,t_1,t_2)$ into a series of powers of $\varepsilon$ as

$$\begin{aligned} y(\tau)&\equiv Y(t_0,t_1,t_2)\\ &=Y_0(t_0,t_1,t_2)+\varepsilon Y_1(t_0,t_1,t_2)\\ &\quad+\varepsilon^2Y_2(t_0,t_1,t_2)+\cdots. \end{aligned} \tag{25a}$$

The delayed term $y(\tau-T_{2o})$ is accordingly written as

$$\begin{aligned} y(\tau-T_{2o})&\equiv Y\big(t_0-T_{2o},t_1-\varepsilon T_{2o},t_2-\varepsilon^2T_{2o}\big)\\ &=Y_0\big(t_0-T_{2o},t_1-\varepsilon T_{2o},t_2-\varepsilon^2T_{2o}\big)\\ &\quad+\varepsilon Y_1\big(t_0-T_{2o},t_1-\varepsilon T_{2o},t_2-\varepsilon^2T_{2o}\big)\\ &\quad+\cdots. \end{aligned} \tag{25b}$$

Equation (25b) is further expanded into a Taylor series about $\varepsilon=0$. This is finally substituted into (24) along with (25a) and various powers of $\varepsilon$ are collected. The resulting equation at the first order, i.e., $\mathcal{O}(\varepsilon^0)$, is

$$\frac{\partial^2Y_0}{\partial t_0^2}+Y_0-h_1\frac{\partial Y_0}{\partial t_0}=K_{c2o}Y_0(t_0-T_{2o},t_1,t_2), \tag{26}$$

where the explicit dependence on the various time scales has been dropped for brevity. The various time scales have been retained for the delayed term in (26) to clarify the resulting delayed term after the Taylor expansion. The steady-state solution to (26) (from linear analysis) can be written as

$$Y_0=C_1\sin(\omega t_0)+C_2\cos(\omega t_0), \tag{27}$$

where $C_1=C_1(t_1,t_2)$ and $C_2=C_2(t_1,t_2)$. The equation at $\mathcal{O}(\varepsilon)$ after substituting (27) for $Y_0$ is

$$\begin{aligned} &\frac{\partial^2Y_1}{\partial t_0^2}-h_1\frac{\partial Y_1}{\partial t_0}+Y_1-K_{c2o}Y_1(t_0-T_{20})\\ &\quad+P_1\sin(\omega t_0)+P_2\cos(\omega t_0)+P_3\sin(2\omega t_0)\\ &\quad+P_4\cos(2\omega t_0)+P_5=0, \end{aligned} \tag{28}$$

where

$$\begin{aligned} P_1&=\big(-h_1+K_{c2o}T_{2o}\cos(\omega T_{2o})\big)\frac{\partial C_1}{\partial t_1}\\ &\quad-\big(2\omega-K_{c2o}T_{2o}\sin(\omega T_{2o})\big)\frac{\partial C_2}{\partial t_1},\\ P_2&=\big(2\omega-K_{c2o}T_{2o}\sin(\omega T_{2o})\big)\frac{\partial C_1}{\partial t_1}\\ &\quad+\big(-h_1+K_{c2o}T_{2o}\cos(\omega T_{2o})\big)\frac{\partial C_2}{\partial t_1},\\ P_3&=h_2\omega^2C_1C_2,\\ P_4&=-\frac{h_2\omega^2}{2}\big(C_1^2-C_2^2\big),\\ P_5&=-\frac{h_2\omega^2}{2}\big(C_1^2+C_2^2\big). \end{aligned}$$

To avoid secular terms, the coefficients of $\sin(\omega t_0)$ and $\cos(\omega t_0)$ in (28) are set to zero. This gives us $\frac{\partial C_1}{\partial t_1}=0$ and $\frac{\partial C_2}{\partial t_1}=0$. Equation (26) can then be solved for $Y_1$ in the following form:

$$Y_1=C_3+C_4\sin(2\omega t_0)+C_5\cos(2\omega t_0), \tag{29}$$

by considering the particular solution only. The coefficients $C_3$, $C_4$ and $C_5$ can be obtained in terms of the parameters in (28). The results obtained so far, including the expressions $\frac{\partial C_1}{\partial t_1}$ and $\frac{\partial C_2}{\partial t_1}$, are now substituted into the equation at $\mathcal{O}(\varepsilon^2)$. Again there are terms containing $\sin(\omega t_0)$ and $\cos(\omega t_0)$ which can give rise to secular terms. Accordingly, and as before, the coefficients of $\sin(\omega t_0)$ and $\cos(\omega t_0)$ in the $\mathcal{O}(\varepsilon^2)$ equation are set to zero which can then be solved to obtain $\frac{\partial C_1}{\partial t_2}$ and $\frac{\partial C_2}{\partial t_2}$. The above procedure can in principle be continued indefinitely to any order. Finally, the rate of change of $C_1$ and $C_2$ in the original time $\tau$ (up to the second order) is given by

$$C_1'=\frac{\partial C_1}{\partial\tau}=\varepsilon\frac{\partial C_1}{\partial t_1}+\varepsilon^2\frac{\partial C_1}{\partial t_2}+\mathcal{O}\big(\varepsilon^3\big)\quad\text{and}$$

$$C_2'=\frac{\partial C_2}{\partial\tau}=\varepsilon\frac{\partial C_2}{\partial t_1}+\varepsilon^2\frac{\partial C_2}{\partial t_2}+\mathcal{O}\big(\varepsilon^3\big).$$

The actual expressions involved, obtained here using the symbolic algebra package MAPLE, are lengthy and not displayed here. We further change variables to polar coordinates as $C_1(\tau)=R_1(\tau)\cos(\varphi_1(\tau))$ and $C_2(\tau)=R_1(\tau)\sin(\varphi_1(\tau))$. The solution in the original variable becomes $z(\tau)=\varepsilon y(\tau)=A_1(\tau)\times$

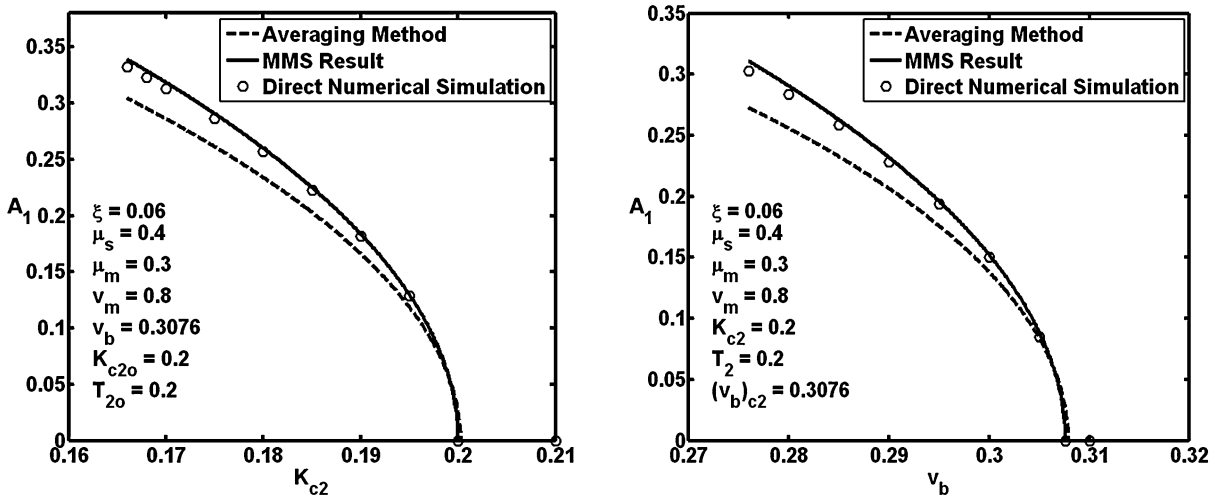


**Fig. 5** Amplitude of pure slipping motion of the mass as a function of (**a**) control gain, (**b**) belt velocity. *Circles* correspond to numerical solution of (6b). *Solid* and *dashed lines* correspond to MMS results and results obtained from the averaging method respectively. $(v_b)_{c2}$ denotes the critical belt velocity for control force 2

$\sin(\tau+\varphi_1(\tau))$, where $A_1(\tau)=\varepsilon R_1(\tau)$. The slow-flow equations governing the evolution of the amplitude and the phase are

$$\frac{dA_1}{d\tau}=(B_1\Delta_1)A_1+B_2A_1^3, \tag{30}$$

$$\frac{d\varphi_1}{d\tau}=(B_3\Delta_1)+B_4A_1^2, \tag{31}$$

where $\Delta_1=\varepsilon^2\Delta$ and

$$B_1=\frac{1}{4}\frac{H_0+H_1\omega+H_2\omega^2+H_3\omega^3+H_4\omega^4+H_5\omega^5}{D_0+D_1\omega+D_2\omega^2+D_3\omega^3+D_4\omega^4+D_5\omega^5+D_6\omega^6},$$

$$B_2=\frac{1}{4}\frac{G_3\omega^3+G_4\omega^4+G_5\omega^5+G_6\omega^6+G_7\omega^7+G_8\omega^8}{D_0+D_1\omega+D_2\omega^2+D_3\omega^3+D_4\omega^4+D_5\omega^5+D_6\omega^6},$$

$$B_3=\frac{1}{4}\frac{U_0+U_1\omega+U_2\omega^2+U_3\omega^3+U_4\omega^4+U_5\omega^5}{D_0+D_1\omega+D_2\omega^2+D_3\omega^3+D_4\omega^4+D_5\omega^5+D_6\omega^6},$$

$$B_4=\frac{1}{4}\frac{W_3\omega^3+W_4\omega^4+W_5\omega^5+W_6\omega^6+W_7\omega^7}{D_0+D_1\omega+D_2\omega^2+D_3\omega^3+D_4\omega^4+D_5\omega^5+D_6\omega^6}.$$

The expressions for $H_0$, $H_1$, $H_2$ etc. are very lengthy and are given in Appendix. The amplitude of the limit cycle from the amplitude equation (30) is

$$A_1=\sqrt{\frac{-B_1\Delta_1}{B_2}}. \tag{32}$$

For the parameter values shown in Fig. 5(a), we get $B_1=-0.0999948$ and $B_2=-0.0295183$ for the amplitude equation. Hence, for the limit cycle to exist we require $\Delta_1<0$ implying $K_{c2}<K_{c2o}$ (the linearly unstable region). Stability analysis of the fixed point (32) of the slow-flow equation (30) gives us that the limit cycle is stable. A stable limit cycle coexisting with an unstable equilibrium implies that the bifurcation is supercritical in nature.

The previous analysis can also be performed by considering the belt velocity $v_b$ as the bifurcation parameter. In this case, we perturb $v_b$ as $v_b=(v_b)_{c2}+\varepsilon^2\Delta$. The relevant equation for this case can be obtained by substituting $h_1=h_{1o}+\varepsilon^2\Delta_{h1}$ and $h_2=h_{2o}+\varepsilon^2\Delta_{h2}$ into (23), where $h_{1o}$ and $h_{2o}$ are the values of $h_1$ and $h_2$ at the critical belt velocity $(v_b)_{c2}$ and $\Delta_{h1}=-\frac{2\alpha_1(v_b)_{c2}}{v_m^2}\Delta$ and $\Delta_{h2}=\frac{\alpha_1}{v_m^2}\Delta$. Following the procedure outlined above, we find the same form of the amplitude and phase equations as given by (31) with $\Delta_1=\varepsilon^2\Delta_{h1}=-\varepsilon^2\frac{2\alpha_1(v_b)_{c2}}{v_m^2}\Delta$. The coefficients in the amplitude equation (30) for parameters in Fig. 5(b) are $B_1=0.501997$ and $B_2=-0.0295183$. The bifurcation diagrams obtained using numerical simulations and the two asymptotic methods considering both $K_{c2}$ and $v_b$ as the bifurcation parameters, are compared in Fig. 5.

A similar analysis for control force 1 (6a) with $K_{c1}$ as the bifurcation parameter and other parameters as shown in Fig. 6(a) gives the coefficients as $B_1=-0.3634388$ and $B_2=0.033795$; and with $v_b$

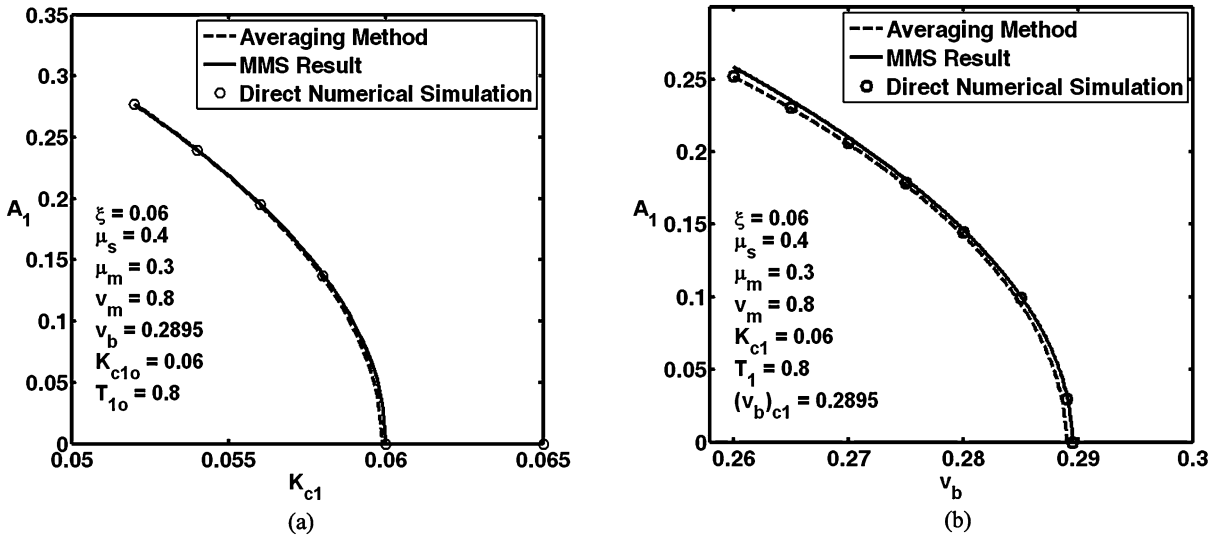


**Fig. 6** Amplitude of pure slipping motion of the mass as a function of (**a**) control gain, (**b**) belt velocity. *Circles* correspond to numerical integration of (6a). *Solid* and *dashed lines* correspond to MMS results and results obtained from the averaging method respectively. $(v_b)_{c1}$ denotes the critical belt velocity for control force 1

as the bifurcation parameter (with other parameters as shown in Fig. 6(b)), we get $B_1 = 0.508729$ and $B_2 = 0.037951$. The corresponding bifurcation diagrams are again compared in Fig. 6.

We observe from Figs. 5 and 6 that the MMS solution approximates the numerical solution better than the results obtained using the averaging method. For control force 1, the results obtained using the averaging method and the MMS are equally good in Fig. 6. This is because of the choice of a smaller time delay where the stability boundary by averaging method almost coincides with the exact stability boundary. For higher time delays, the stability boundary by the averaging method differs significantly from the exact stability boundary and, hence, the MMS result outperforms the averaging method. The inferior performance of the averaging method is again due to the approximation in (16) whereby it holds only for small values of $K_{c1}$.

## 4 Analysis of the system with exponential friction model

In this section, we will analyze the system with the exponential friction model. Since majority of the analysis follows almost exactly as in Sect. 3, only the salient features of the approach are presented here and we focus more on the results.

### 4.1 Linear stability analysis

The linearized form of (8a) and (8b) is exactly similar to (9a) and (9b) with $h_1 = \gamma a - 2\xi$. Details of the subsequent analysis are, therefore, suppressed and only the results are plotted in Fig. 7.

As noted previously, the stability regimes increase with an increase in the belt velocity. In the next subsection, we perform the nonlinear analysis using the method of multiple scales (MMS) only. The averaging method has not been reported as it does not provide any new information and has been already shown to be inferior to MMS in Sect. 3.

### 4.2 Nonlinear analysis by method of multiple scales (MMS)

We substitute $z = \varepsilon y$ into (8a) (for control force 1) to render the nonlinearities small, and then expand the exponential term in a series and retain only terms up to the third order to obtain

$$y'' + y - h_1 y' - \varepsilon h_2 y'^2 - \varepsilon^2 h_3 y'^3 + K_{c1} y(\tau) - K_{c1} y(\tau - T_1) = 0 \tag{33}$$

with $h_1 = \gamma a - 2\xi$, $h_2 = \frac{\gamma a^2}{2}$, $h_3 = \frac{\gamma a^3}{6}$ and $\gamma = (\Delta\mu)e^{-av_b}$. Proceeding as in Sect. 3.2.2, we obtain the

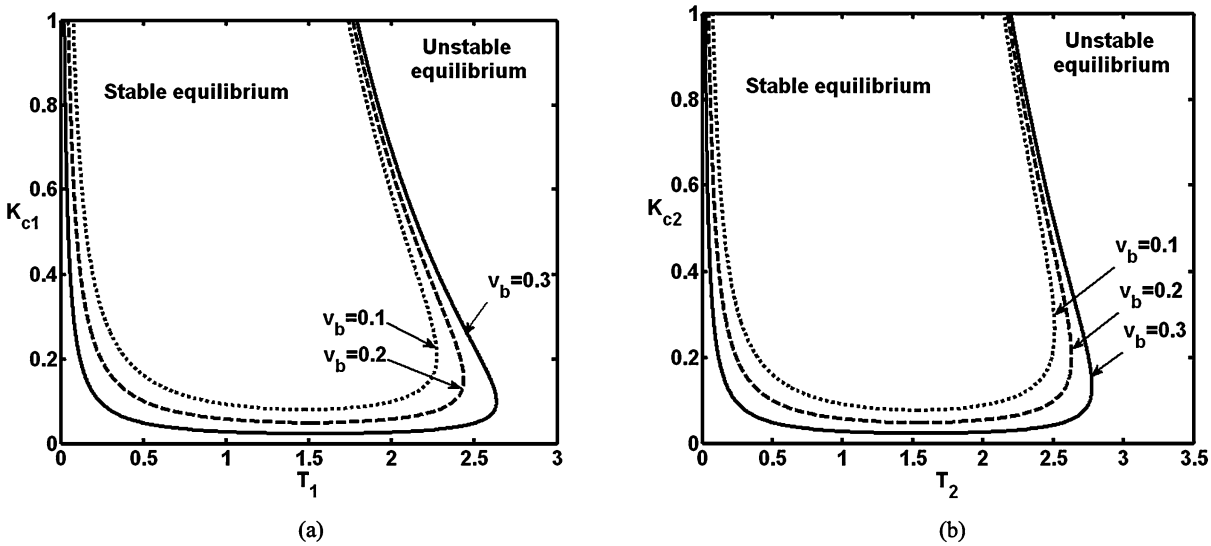


**Fig. 7** Stability boundaries for (**a**) control force 1 and (**b**) control force 2. Parameters: $\xi = 0.06$, $\mu_k = 0.4$, $\mu_k = 0.255$, $a = 1.6$

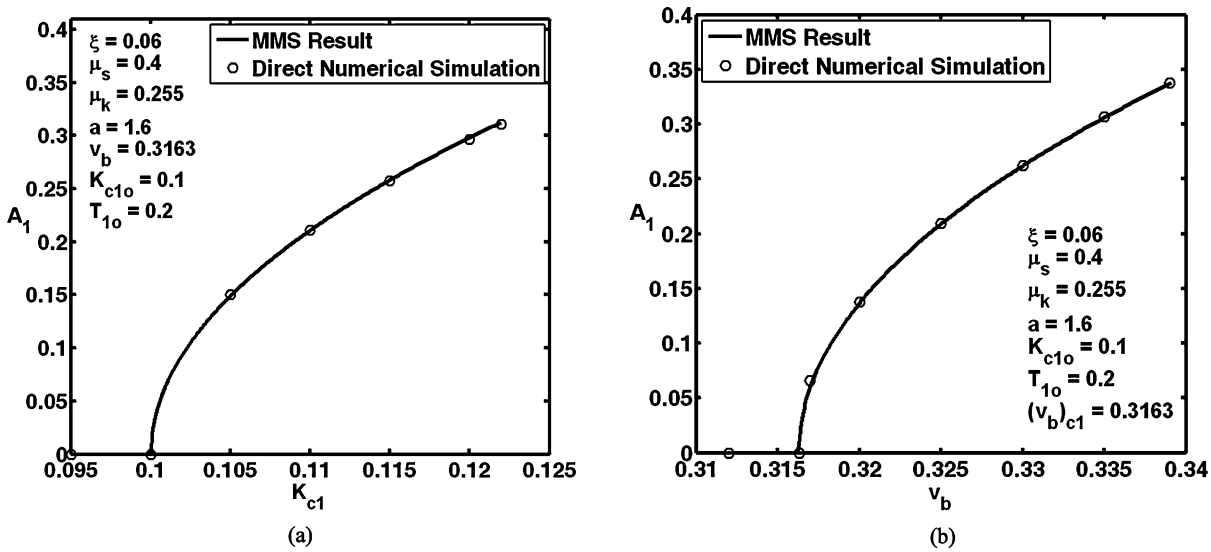


**Fig. 8** Amplitude of unstable limit cycle as a function of (**a**) control gain, (**b**) belt velocity. *Circles* correspond to numerical solution of (8a). *Solid line* corresponds to MMS results. $(v_b)_{c1}$ denotes the critical belt velocity

amplitude and phase equations which have the same form as given by (30) and (31), i.e.,

$$\frac{dA_1}{d\tau} = (B_1\Delta_1)A_1 + B_2A_1^3,$$

$$\frac{d\varphi_1}{d\tau} = (B_3\Delta_1) + B_4A_1^2.$$

For the parameter values shown in Fig. 8(a), we get $B_1 = -0.1976153565$ and $B_2 = 0.8242027821$ for the amplitude equation with the control gain $K_{c1}$ as the bifurcation parameter. Note from the values of $B_1$ and $B_2$ that for a limit cycle to exist, we require $\Delta_1 > 0$, which implies $K_{c1} > K_{c1o}$ (the linearly stable region). A linear stability analysis of the fixed point corresponding to this limit cycle reveals that it is unstable. Hence, an unstable limit cycle coexists with a stable equilibrium, signifying a subcritical bifurcation.

While considering the belt velocity $v_b$ as the bifurcation parameter, we perturb $v_b$ as $v_b = (v_b)_{c1} + \varepsilon^2 \Delta$. Accordingly, $h_1$, $h_2$ and $h_3$ get modified to $h_1 = h_{1o} + \varepsilon^2 \Delta_{h1}$, $h_2 = h_{2o} + \varepsilon^2 \Delta_{h2}$ and $h_3 = h_{3o} + \varepsilon^2 \Delta_{h3}$, where $h_{1o}$, $h_{2o}$ and $h_{3o}$ are the values of $h_1$, $h_2$ and $h_3$ at the critical belt velocity $(v_b)_{c1}$, and $\Delta_{h1} = -((\Delta\mu)a^2 e^{-a(v_b)_{c1}})\Delta$, $\Delta_{h2} = -(\frac{(\Delta\mu)a^3}{2} e^{-a(v_b)_{c1}})\Delta$ and $\Delta_{h3} = -(\frac{(\Delta\mu)a^4}{6} e^{-a(v_b)_{c1}})\Delta$. The coefficients of the amplitude equations are $B_1 = 0.507905784$ and $B_2 = 0.8242027821$ for the parameter values shown in Fig. 8(b), with $\Delta_1 = \varepsilon^2 \Delta_{h1} = -\varepsilon^2((\Delta\mu)a^2 e^{-a(v_b)_{c1}})\Delta$. Again, the bifurcation is subcritical in nature and unstable limit cycles exist around the stable equilibrium for $v_b > (v_b)_{c1}$.

As expected, the MMS result matches the numerical results very well. Note that there are large amplitude limit cycles involving stick-slip motion coexisting with the small-amplitude unstable limit cycles. These stick-slip limit cycles are not shown in Fig. 8. These solutions involving stick-slip motion require special analytical as well as numerical techniques which are not explored in this paper. However, the limiting case wherein the stable stick-slip motion coincides with the unstable pure slip motion is considered in the next section for the global stability analysis. This analysis is required to obtain the critical velocity corresponding to global stability of the static equilibrium since it is only locally stable above the critical belt velocity due to the subcritical nature of the bifurcation.

### 4.3 Global stability analysis

The analysis in this section closely follows the corresponding analysis in [31]. The unstable limit cycle merges with the stable stick-slip limit cycle in a cyclic fold bifurcation leaving the static equilibrium globally stable afterwards. At the cyclic fold point, there is a unique limit cycle which is tangential to the $v_r = 0$ line, or equivalently, tangential to the $z' = v_b$ line in the $z$–$z'$ plane. Hence, the solutions to (8a) and (8b) can be written as

$$\begin{aligned} z' &= v_b \cos(\omega\tau), \quad \text{and} \\ z &= c_0 + \tfrac{v_b}{\omega} \sin(\omega\tau), \end{aligned} \tag{34}$$

where the constant $c_0$ can be obtained using harmonic balance. However, it is not important for the current analysis. The frequency of oscillation $\omega$ in (34) is either $\omega_1$ or $\omega_2$, depending on the control force. The equations relating the frequencies $\omega_1$ and $\omega_2$ with the control parameters (found using harmonic balance method) are

$$\omega_1^2 - (1 + K_{c1}) + K_{c1} \cos(\omega_1 T_1) = 0, \tag{35a}$$

$$\omega_2^2 - 1 + K_{c2} \cos(\omega_2 T_2) = 0, \tag{35b}$$

respectively. The change in energy per cycle at the cyclic fold point for these two cases is given by

$$\mathrm{E}_1(K_{c1}, T_1) = \frac{\pi v_b}{\omega_1}\left(2\gamma I_1(a v_b) - 2\xi v_b - \frac{v_b K_{c1}}{\omega_1} \sin(\omega_1 T_1)\right), \tag{36a}$$

$$\mathrm{E}_2(K_{c2}, T_2) = \frac{\pi v_b}{\omega_2}\left(2\gamma I_1(a v_b) - 2\xi v_b - \frac{v_b K_{c2}}{\omega_2} \sin(\omega_2 T_2)\right) \tag{36b}$$

with $I_1(a v_b)$ as the modified Bessel's functions of order one. For a limit cycle, the change in energy per cycle is zero and accordingly $\mathrm{E}_1 = 0$ and $\mathrm{E}_2 = 0$. This condition, along with (35a) and (35b), gives us the required equations for the global stability boundary for the two control forces. These can be solved to either get the belt velocities $(v_b)_{g1}$ and $(v_b)_{g2}$ corresponding to the cyclic fold point for fixed values of control parameters, or the values of the control parameters for a given belt velocity. The global stability boundary in the control parameter plane thus obtained is shown in Fig. 9, along with the linear stability boundary for both the control forces.

In the next section, we will compare the efficacy of the two types of time-delayed control forces in quenching friction-induced oscillations.

## 5 Comparison of the control forces

The comparison in this section is mainly based on the stability of the static equilibrium, which implies complete quenching of the vibrations. However, partial quenching with only a reduction in the amplitude is also considered as another criterion wherein the effect of the two control forces is compared based on the bifurcation diagrams. Finally, some comparison has been done based on the control energy and control force requirements. The choice of friction parameters

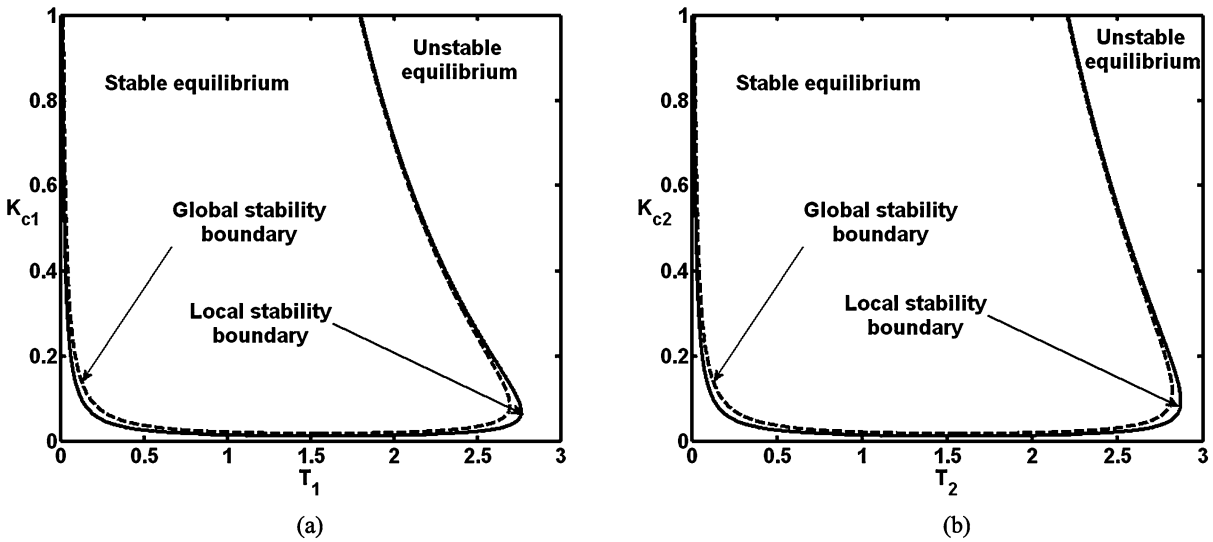


**Fig. 9** Local and global stability boundaries in the control parameter plane for (**a**) control force 1, (**b**) control force 2. Parameters are: $v_b = 0.35$, $\xi = 0.06$, $\mu_s = 0.4$, $\mu_k = 0.255$ , and $a = 1.6$

in the previous sections was governed by the fact that the two friction forces match reasonably well in the desired interval of relative velocities. This was done to highlight the fact that two similarly looking friction models can give rise to different qualitative nature of the bifurcation. In this section, we will use a different set of friction parameters to accentuate the difference between the two control forces. We also emphasize that this paper is completely based on theoretical considerations. Implementation of these control forces in an experimental study will involve several practical considerations which might require fine-tuning of certain control parameters and could possibly give rise to observations which are in conflict with the current paper. However, we expect the trends to largely remain the same. Detailed experimental study along these lines will be carried out in future.

### 5.1 Comparison based on complete quenching of vibrations

Figure 10 compares the stability boundaries for control forces 1 and 2 for the two different friction models (or equivalently, two different sets of system parameters). It is observed that the stability region for control force 2 is larger than that for the control force 1 in both the cases (for $K_c < 1$).[1] This implies that for the same control gain, the static equilibrium is stable for a larger range of time delays for the control force 2 implying higher robustness of control w.r.t. fluctuations in the time delay. The same holds for a variation in the control gain for a fixed time delay as long as the control gain is smaller than 1.

Figure 11 compares the critical belt velocity for the two control forces for the system with the polynomial friction model. The critical belt velocity is found from the linear stability analysis as described in Sect. 3.1 (i.e., (15a) and (15b)), and above the critical belt velocity the static equilibrium is globally stable since the bifurcation is supercritical in nature. It is observed that the critical belt velocity for control force 2 is always less than that for control force 1 for all control gains and delays. The critical belt velocities for the two forces are very close to each other for smaller delays and the difference increases with an increase in the delay. The critical belt velocities are the smallest in the intermediate delay regime and, hence, we will focus on this regime in the hardware implementation of the control forces. Control force 2 clearly has a significantly smaller minimum critical belt velocity than control force 1. The difference between the two forces

[1] As noted earlier, we do not emphasize on larger control gains since the objective of vibration quenching can be achieved with smaller control gains as well.

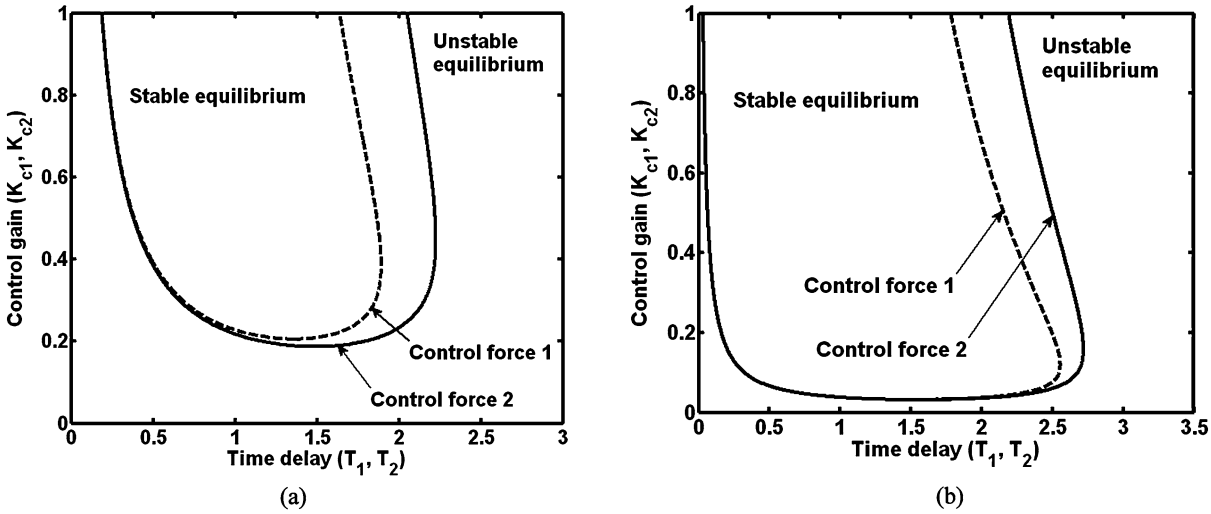


**Fig. 10** Comparison of stability boundaries for control forces 1 and 2. (**a**) For polynomial friction model with parameters $v_b = 0.3$, $\xi = 0.05$, $\mu_s = 0.4$, $\mu_m = 0.25$, $v_m = 0.5$. (**b**) For exponential friction model with parameters $v_b = 0.25$, $\xi = 0.025$, $\mu_k = 0.1$, $\Delta\mu = 0.1$, $a = 10$

increases with an increase in the control gain as well. For higher control gains, the critical belt velocity is zero for a range of time delays which means that the system is globally stable for any operating belt velocity. It is also interesting to note that the critical belt velocity for higher time delays increases past the critical belt velocity for the uncontrolled system. Hence, a larger time delay in the control force destabilizes the stable equilibrium.

The critical belt velocities corresponding to the Hopf bifurcation point $(v_b)_c$ and the cyclic fold bifurcation point $(v_b)_g$ for the two types of control forces are compared for ranges of time delays for some fixed values of control gains for the exponential friction model in Fig. 12. Note that the equilibrium is globally stable past $(v_b)_g$ only and is only locally stable past $(v_b)_c$. The difference in the critical belt velocities ($(v_b)_{c1}$ and $(v_b)_{c2}$) for the two control forces and the belt velocities corresponding to the cyclic fold point ($(v_b)_{g1}$ and $(v_b)_{g2}$) follows the same trend as in Fig. 11 for the polynomial friction model. On the other hand, the difference between $(v_b)_{c1}$ and $(v_b)_{g1}$ or $(v_b)_{c2}$ and $(v_b)_{g2}$ starts off at a higher value, reduces with increasing time delays, reaches a minimum for a certain delay value and increases thereafter. Note that this difference is significantly smaller for a large range of control parameters than the difference for the uncontrolled system. Hence, the region of bi-stability is narrowed by time-delayed control forces giving another indication of the effectiveness of control. With an increase in the gain value, the minimum difference between $(v_b)_c$ and $(v_b)_g$ reduces and beyond a certain critical gain value, the two curves almost coincide for certain regimes of the time delays. This roughly means that the equilibrium is globally stable past the Hopf bifurcation point. Also for significantly higher gains, as in Fig. 14(d), the system becomes globally stable for any operating belt velocity for a large range of time delays. In all the four cases, $(v_b)_{c2} < (v_b)_{c1}$ and $(v_b)_{g2} < (v_b)_{g1}$. Hence, control force 2 outperforms control force 1 for the exponential friction model as well.

### 5.2 Comparison based on partial quenching of vibrations

Figure 13 depicts the bifurcation diagram for the polynomial friction model with the belt velocity as the bifurcation parameter for the uncontrolled system, an undelayed linear position feedback and the two delayed feedback control forces. Below the critical belt velocity, the static equilibrium is unstable and there are stable limit cycles. As mentioned earlier, only limit cycles with pure slip motion are plotted in Fig. 13. It is observed from the figure that linear undelayed position feedback reduces the amplitude of oscillations but has no effect on the critical belt velocity. Therefore,

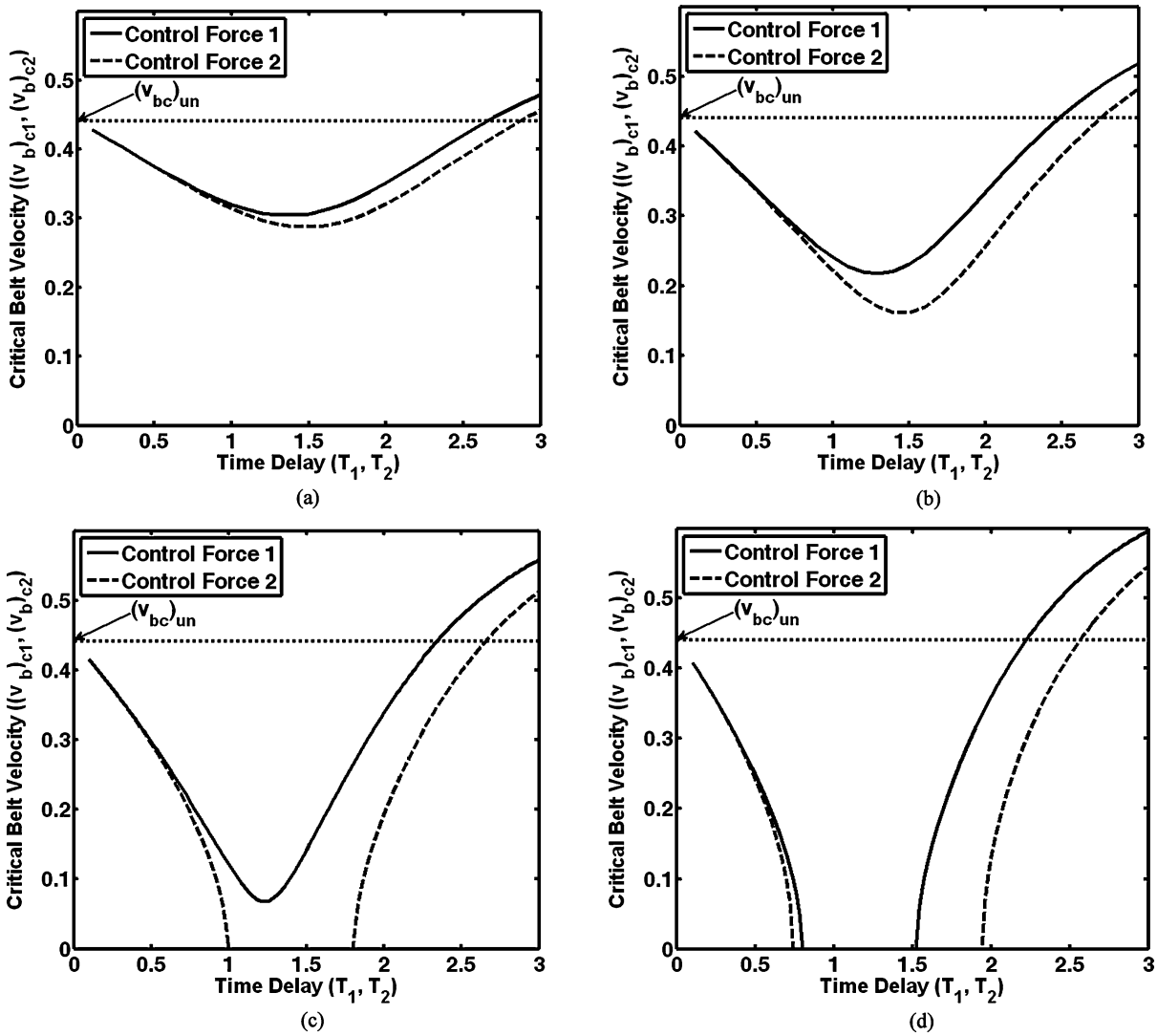


**Fig. 11** Comparison of critical belt velocities for the two types of control forces with the polynomial friction model. $(v_{bc})_{un}$ is the critical belt velocity for the uncontrolled system. Parameters: $\xi = 0.05$, $\mu_s = 0.4$, $\mu_m = 0.25$, $v_m = 0.5$, (**a**) $K_{c1} = K_{c2} = 0.2$, (**b**) $K_{c1} = K_{c2} = 0.3$, (**c**) $K_{c1} = K_{c2} = 0.4$, (**d**) $K_{c1} = K_{c2} = 0.5$

complete quenching of friction-induced vibrations requires time-delayed position feedback.[2] Figure 13(a) is plotted for a time delay of 0.4 for which the critical belt velocities for the two control forces are almost the same (see Fig. 11(a)). It can be noted from Fig. 13(a) that the amplitude of the limit cycles increases faster for control force 2 than that for control force 1. Hence, for this choice of time delay, control force 1 is a better option since for a given belt velocity and control gain, it will result in smaller amplitudes of vibrations. However, for a higher time delay like 1.5 in Fig. 13(b), the critical belt velocity for the control force 2 is lower than that for control force 1. Therefore, for a given belt velocity the amplitude of the limit cycle is always smaller for control force 2. Hence, control force 2 is a better choice even with regard to partial quenching of vibrations.

[2]Note that complete quenching can be attained using undelayed velocity feedback as well. However, the discussions in this paper pertain to position feedback only.

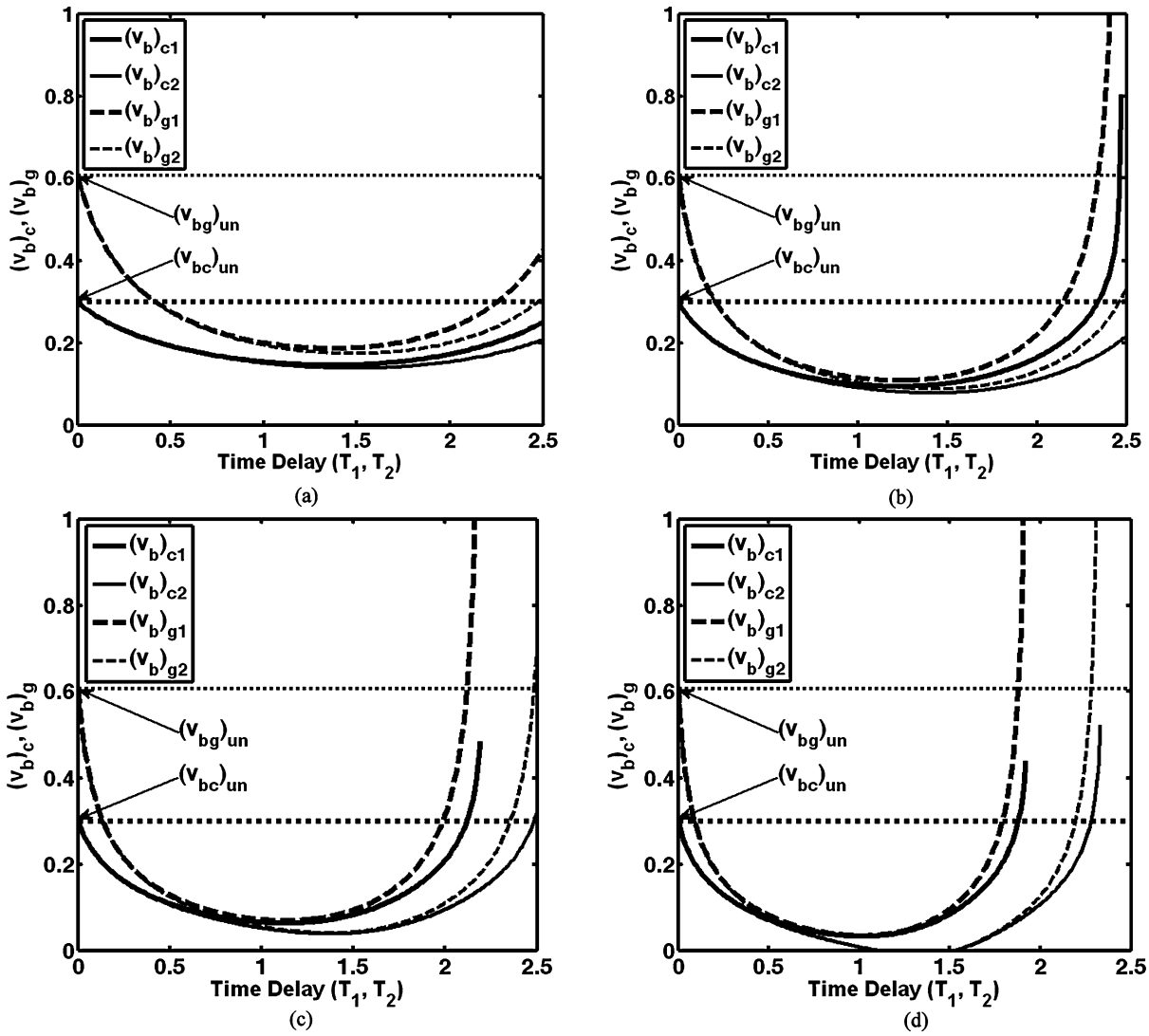


**Fig. 12** Comparison of critical belt velocities corresponding to the Hopf point and the cyclic fold point for the two types of control forces for the exponential friction model. $(v_{bc})_{un}$ and $(v_{bg})_{un}$ are the critical belt velocities corresponding to the Hopf point and the cyclic fold point for the uncontrolled system, respectively. Parameters: $\xi = 0.025$, $\mu_k = 0.1$, $\Delta\mu = 0.1$, $a = 10$, (**a**) $K_{c1} = K_{c2} = 0.2$, (**b**) $K_{c1} = K_{c2} = 0.4$, (**c**) $K_{c1} = K_{c2} = 0.6$, (**d**) $K_{c1} = K_{c2} = 0.9$

Figure 14 shows the same diagrams as in Fig. 13 but for the system with an exponential friction model. Since the bifurcation is subcritical in nature for this friction model, unstable limit cycles coexist with linearly stable equilibrium. In this region of local stability, the equilibrium is stable for perturbations smaller in magnitude than the amplitudes of the limit cycles and unstable for larger perturbations. Hence, it is desirable to have larger amplitude limit cycles for any belt velocity. The unstable limit cycles are plotted up to the cyclic fold bifurcation point after which the static equilibrium is globally stable. It can be observed from Fig. 14(a) and (b), that the amplitudes of the limit cycles are always larger for control force 2 for any given belt velocity. Therefore, equilibrium is stable for larger perturbations for the system with control force 2 than control force 1. Hence, control force 2 outperforms control force 1 for the exponential friction model.

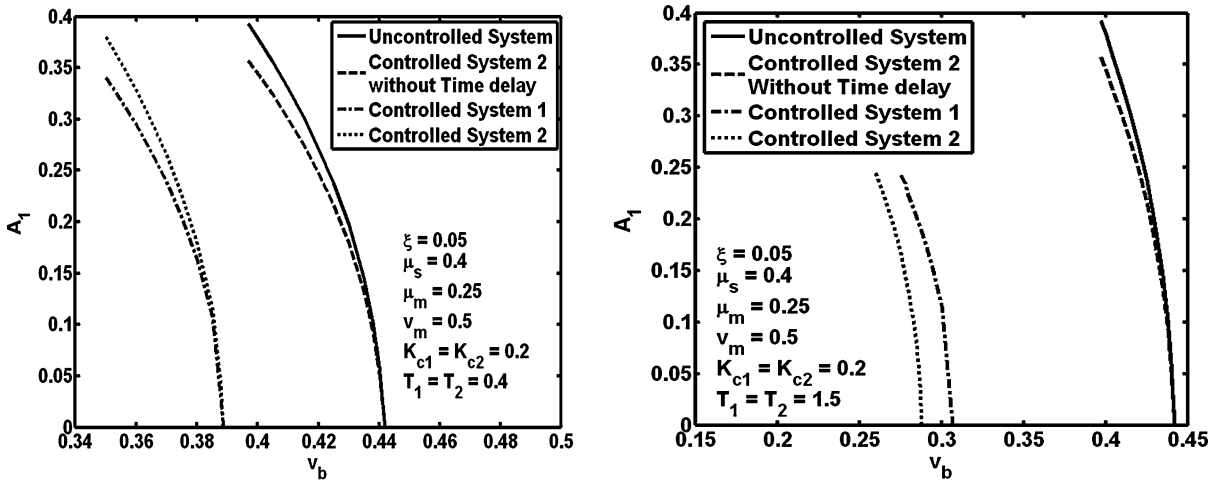


**Fig. 13** Comparison of bifurcation diagrams with belt velocity as the bifurcation parameter for two different sets of parameter values for the polynomial friction model

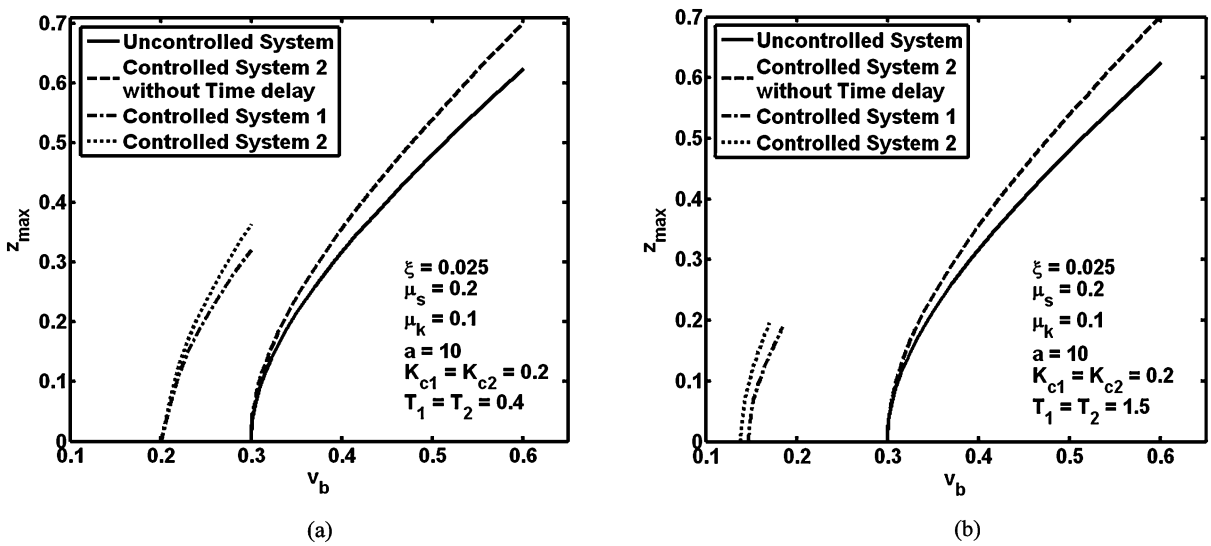


**Fig. 14** Comparison of bifurcation diagrams with belt velocity as the bifurcation parameter for two different sets of parameter values for the exponential friction model

### 5.3 Comparison based on energy and force requirements

In this subsection, we compare the two delayed control strategies considering the required energy and the maximum control force. For this purpose, we consider the operating belt velocity in the unstable regime of the uncontrolled system and control parameters in the stable regime. Therefore, the application of the control force completely quenches the vibrations. For energy calculations, we will consider the energy required to bring the solution to 1% of its amplitude. From (30) (the slow-flow amplitude equation), we get the evolution of the amplitude as

$$A_1(\tau) = \sqrt{\frac{B_1 B_5 \Delta_1 e^{2B_1\Delta_1\tau}}{1 + B_2 B_5 e^{2B_1\Delta_1\tau}}}, \tag{37}$$

where $B_5 = \frac{A_{10}^2}{B_1\Delta_1 - B_2 A_{10}^2}$, $A_{10} = A_1(0)$ is the amplitude of the limit cycle of the uncontrolled system at the operating belt velocity, and other parameters are as explained in Sects. 3.2.2 and 4.2. Now, the energy required to drive the controllers for the two control forces are

$$E_1 = -\int K_{c1}\big[z(\tau - T_1) - z(\tau)\big]z'(\tau)\,d\tau, \tag{38}$$

$$E_2 = -\int K_{c2} z(\tau - T_2) z'(\tau)\,d\tau. \tag{39}$$

To get the energy expressions, we make the following assumptions:

$$\begin{aligned} z(\tau) &= A_1(\tau)\cos(\omega_{1,2}\tau), \\ z'(\tau) &= A_1'(\tau)\cos(\omega_{1,2}\tau) \\ &\quad - \omega_{1,2}A_1(\tau)\sin(\omega_{1,2}\tau), \\ A_1(\tau - T_{1,2}) &= A_1(\tau), \end{aligned} \tag{40}$$

where $\omega_1$ and $\omega_2$ are chosen to be the values obtained from the linear stability analysis of control forces 1 and 2, respectively. With the help of these assumptions and (37) we find the energy expressions as

$$\begin{aligned} E_1(\tau) = &-\frac{K_{c1}B_1B_5\Delta_1 e^{2B_1\Delta_1\tau}}{1 + B_2B_5e^{2B_1\Delta_1\tau}}\cos(\omega_1\tau) \\ &\times \sin\left(\frac{\omega_1 T_1}{2}\right)\sin\left(\omega_1\tau - \frac{\omega_1 T_1}{2}\right) \\ &+ \frac{K_{c1}\omega_1\sin(\omega_1 T_1)\ln(1 + B_2B_5e^{2B_1\Delta_1\tau})}{4B_2} \\ &+ B_6, \end{aligned} \tag{41}$$

$$\begin{aligned} E_2(\tau) = &\frac{K_{c2}B_1\Delta_1\cos(\omega_2 T_2)}{2B_2(1 + B_2B_5e^{2B_1\Delta_1\tau})} \\ &+ \frac{K_{c2}B_1B_5\Delta_1 e^{2B_1\Delta_1\tau}}{2(1 + B_2B_5e^{2B_1\Delta_1\tau})} \\ &\times \sin(\omega_2\tau)\sin(\omega_2\tau - \omega_2 T_2) \\ &+ \frac{K_{c2}\omega_2\sin(\omega_2 T_2)\ln(1 + B_2B_5e^{2B_1\Delta_1\tau})}{4B_2} \\ &+ B_7. \end{aligned} \tag{42}$$

The integration constants $B_6$ and $B_7$ are obtained by imposing $E_1(0) = 0$ and $E_2(0) = 0$.

The expressions for energy ((41) and (42)) are obtained using the assumption $A_1(\tau - T_{1,2}) = A_1(\tau)$ and are, therefore, valid either for smaller time delays only or when the system is close to the Hopf point such that the amplitude varies slowly with time. The energy required for the two control forces considering the polynomial friction model with system parameters $\xi = 0.05$, $\mu_s = 0.4$, $\mu_m = 0.25$, $v_m = 0.5$, $v_b = 0.4$, $T_1 = T_2 = 1.5$ is shown in Fig. 15. To generate this figure, first (37) is solved for the time required for the amplitude to become 0.1 $A_{10}$ and this value is then substituted into (41) or (42) for control forces 1 and 2, respectively. It can be seen from Fig. 15 that for a fixed time delay, control force 2 requires lesser energy than control force 1 for smaller control gains and the scenario reverses for higher control gains.

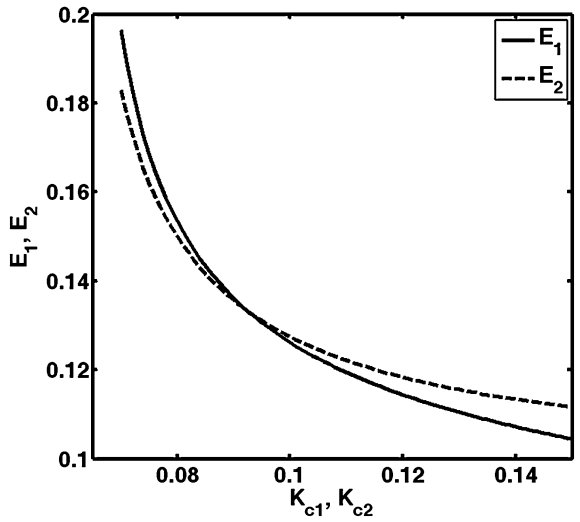


**Fig. 15** Energy required for the two control forces for the polynomial friction model with parameters $\xi = 0.05$, $\mu_s = 0.4$, $\mu_m = 0.25$, $v_m = 0.5$, $v_b = 0.4$, $T_1 = T_2 = 1.5$

We next consider the maximum force required by the two control forces. Control forces 1 and 2 with the assumptions given in (40) give us

$$F_1 = K_{c1}A_1(\tau)\big[\cos(\omega_1\tau - \omega_1 T_1) - \cos(\omega_1\tau)\big] \quad \text{and}$$
$$F_2 = K_{c2}A_1(\tau)\cos(\omega_2\tau - \omega_2 T_2).$$

Clearly the maximum value of $A_1(\tau)$ is $A_{10}$. Substituting this into the above equations and taking the maximum of the other time-dependent terms, we get

$$\begin{aligned} (F_1)_{\max} &= 2K_{c1}A_{10}\sin\left(\frac{\omega_1 T_1}{2}\right) \quad \text{and} \\ (F_2)_{\max} &= K_{c2}A_{10}. \end{aligned} \tag{43}$$

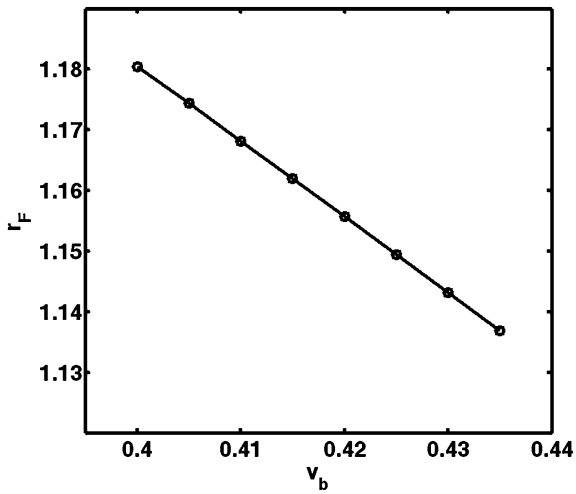


**Fig. 16** Ratio of maximum forces required for the two control forces as a function of the belt velocity. Parameters: $\xi = 0.05$, $\mu_s = 0.4$, $\mu_m = 0.25$, $v_m = 0.5$, $T_1 = T_2 = 1.2$

From (43), we note that the maximum control force is linearly proportional to the control gain for a fixed value of the time delay. Accordingly, to minimize the maximum control force along with achieving the objective of stabilization of the equilibrium, we choose the control gains at the Hopf point. The ratio of the minimum values of these maximum control forces can then be obtained as

$$r_F = 2\frac{K_{c1o}}{K_{c2o}}\sin\left(\frac{\omega_1 T_1}{2}\right). \tag{44}$$

Thus, the maximum force ratio depends largely on the time delay $T_1$ and to a smaller extent on the belt velocity via the frequency $\omega_1$ at the Hopf point. It is observed from Fig. 10(a) that for a fixed belt velocity and time delay, $K_{c1o} > K_{c2o}$. Also from (13a), we must have $\omega_1 > 1$ for $K_{c1} > 0$. Thus, if the time delay is chosen such that $T_1 > \frac{\pi}{3}$, we always will get $r_F > 1$ (as depicted in Fig. 16). Note from Fig. 10(a) that the region around $T_1 > \frac{\pi}{3}$ is the region corresponding to the minimum control gain as well and, hence, is the preferred choice for minimization of the control forces. Therefore, from the point of view of the minimum control force required for stabilization, the control strategy of $K_{c2}z(\tau - T_2)$ seems to be the preferred choice as well.

## 6 Conclusions

In this paper, we have performed a detailed study on the effectiveness of time-delayed control forces for friction-induced vibrations. Two different models for the frictional forces which are popular in the literature have been considered and shown to result in qualitatively different dynamics. Two different control strategies based on time-delayed feedback from previous literature have also been considered. Both linear and nonlinear stability analysis is performed. Stability boundaries separating regions with stable and unstable equilibria are plotted in the plane of the control parameters (control gain and time delay). Stability is found to be lost via a Hopf bifurcation. Nonlinear analysis is performed using two different perturbation methods, viz. the method of averaging and the method of multiple scales (MMS). It has been observed that the method of multiple scales requires less approximation than the method of averaging and is, therefore, superior in the sense that the results obtained from MMS match the numerical solution much better.

It has been found that the nature of the Hopf bifurcation depends on the specific friction model used in the analysis. In particular, the bifurcation is supercritical for the polynomial friction model used by Thomsen [4] while it is subcritical for the exponential friction model used by Hinrichs et al. [3]. The friction parameters for the two models were chosen such that the frictional forces represented by the two models closely match in a certain range of relative velocity. However, they differed in the sign of the third derivative of the force w.r.t. the relative velocity. Hence, a set of experimental data points for the friction force versus relative velocity can be fitted with any one of the two friction models; but the system dynamics, i.e., the nature of the bifurcation, will depend on the model. The model to be used for these vibrations under given operating conditions, therefore, should be obtained using an experimental investigation of the nature of the associated bifurcation. We will perform this study in our future work.

Our comparison of the two types of control forces derived from time-delayed feedback shows that theoretically the control force given by $K_c z(\tau - T)$ is more desirable than the control force $K_c[z(\tau - T) - z(\tau)]$ in almost all measures of control effectiveness used in this study. The various measures of effectiveness used for comparison of the control forces include complete and partial quenching of the vibrations as well as energy and maximum force requirements. Detailed experimental investigation required to verify these observations will be performed in future.

**Acknowledgements** We thank Professor A.K. Mallik for useful technical discussions. We also thank the anonymous reviewers for their constructive comments. We further thank Department of Science and Dechnology (DST), India for financial support.

## Appendix: Expressions involved in the slow-flow equations, i.e., (30) and (31)

$$
\begin{aligned}
H_0 &= 4T_{2o}K_{c2o}^3 + 4\cos(3\omega T_{2o})h_1K_{c2o} + 4T_{2o}K_{c2o} \\
&\quad - 8\cos(2\omega T_{2o})T_{2o}K_{c2o}^2 - 4\cos(\omega T_{2o})h_1 \\
&\quad - 4\cos(\omega T_{2o})h_1K_{c2o}^2 + 4\cos(\omega T_{2o})h_1K_{c2o}, \\
H_1 &= -16\sin(2\omega T_{2o})T_{2o}K_{c2o}^2h_1 \\
&\quad + 8\sin(3\omega T_{2o})h_1^2K_{c2o} + 8\sin(3\omega T_{2o})K_{c2o} \\
&\quad - 8\sin(\omega T_{2o}) - 8\sin(\omega T_{2o})K_{c2o}^2 \\
&\quad - 8\sin(\omega T_{2o})K_{c2o}^2 + 8\sin(\omega T_{2o})h_1^2K_{c2o}, \\
H_2 &= -32T_{2o}K_{c2o} + 32\cos(2\omega T_{2o})T_{2o}K_{c2o}^2 \\
&\quad + 16T_{2o}K_{c2o}h_1^2 - 32\cos(3\omega T_{2o})h_1K_{c2o} \\
&\quad + 32\cos(\omega T_{2o})h_1 - 16\cos(\omega T_{2o})h_1^3, \\
H_3 &= -32\sin(3\omega T_{2o})K_{c2o} - 32\sin(\omega T_{2o})h_1^2 \\
&\quad + 32\sin(\omega T_{2o})K_{c2o} + 64\sin(\omega T_{2o}), \\
H_4 &= 64T_{2o}K_{c2o} - 64\cos(\omega T_{2o})h_1, \\
H_5 &= -128\sin(\omega T_{2o}),\ G_3 = 3T_{2o}K_{c2o}^2\sin(\omega T_{2o})h_3 \\
&\quad - 3\sin(3\omega T_{2o})T_{2o}K_{c2o}^2h_3 \\
&\quad + 3T_{2o}K_{c2o}\sin(\omega T_{2o})h_3 \\
&\quad + 3T_{2o}K_{c2o}^3\sin(\omega T_{2o})h_3, \\
G_4 &= 6T_{2o}K_{c2o}^2h_3\cos(\omega T_{2o})h_1 \\
&\quad - 12\cos(2\omega T_{2o})h_3K_{c2o} \\
&\quad - 4\cos(2\omega T_{2o})h_1h_2^2K_{c2o} \\
&\quad - 4T_{2o}K_{c2o}\cos(\omega T_{2o})h_2^2 \\
&\quad + 4\cos(3\omega T_{2o})T_{2o}K_{c2o}^2h_2^2 \\
&\quad - 6\cos(3\omega T_{2o})T_{2o}K_{c2o}^2h_3h_1 \\
&\quad + 6h_3 + 4h_1h_2^2 + 6h_3K_{c2o}^2, \\
G_5 &= -12\sin(3\omega T_{2o})T_{2o}K_{c2o}^2h_3 \\
&\quad - 12T_{2o}K_{c2o}\sin(\omega T_{2o})h_1^2h_3 \\
&\quad + 8\sin(2\omega T_{2o})h_2^2K_{c2o} \\
&\quad - 24\sin(2\omega T_{2o})h_3K_{c2o}h_1 \\
&\quad + 24T_{2o}K_{c2o}\sin(\omega T_{2o})h_3 \\
&\quad + 8T_{2o}K_{c2o}\sin(\omega T_{2o})h_2^2h_1 \\
&\quad + 12T_{2o}K_{c2o}^2\sin(\omega T_{2o})h_3, \\
G_6 &= 16T_{2o}K_{c2o}\sin(\omega T_{2o})h_2^2 + 48\cos(2\omega T_{2o})h_3K_{c2o} \\
&\quad - 32h_1h_2^2 + 24h_3h_1^2 - 48h_3, \\
G_7 &= -48T_{2o}K_{c2o}\sin(\omega T_{2o})h_3, \\
G_8 &= 96h_3, \\
U_0 &= 4\sin(\omega T_{2o})h_1K_{c2o} + 4\sin(\omega T_{2o})h_1 \\
&\quad - 4\sin(3\omega T_{2o})h_1K_{c2o} + 4\sin(\omega T_{2o})h_1K_{c2o}^2, \\
U_1 &= 8\cos(3\omega T_{2o})K_{c2o} + 8\cos(3\omega T_{2o})K_{c2o} \\
&\quad - 8\cos(\omega T_{2o})K_{c2o}^2 - 8\cos(\omega T_{2o})h_1^2K_{c2o} \\
&\quad - 8\cos(\omega T_{2o}) + 8\cos(3\omega T_{2o})h_1^2K_{c2o}, \\
U_2 &= -32h_1\sin(\omega T_{2o}) + 32\sin(3\omega T_{2o})h_1K_{c2o} \\
&\quad + 16\sin(\omega T_{2o})h_1^3, \\
U_3 &= -32\cos(\omega T_{2o})h_1^2 - 32\cos(\omega T_{2o})K_{c2o} \\
&\quad + 64\cos(\omega T_{2o}) - 32\cos(3\omega T_{2o})K_{c2o}, \\
U_4 &= 64\sin(\omega T_{2o})h_1,\ U_5 = -128\cos(\omega T_{2o}), \\
W_3 &= -3K_{c2o}^2h_1h_3 - 3T_{2o}K_{c2o}^2\cos(\omega T_{2o})h_3 \\
&\quad - 3h_1h_3 + 3T_{2o}K_{c2o}\cos(\omega T_{2o})h_3 \\
&\quad + 3\cos(\omega T_{2o})T_{2o}K_{c2o}^3h_3 \\
&\quad - 3T_{2o}K_{c2o}^2\cos(3\omega T_{2o})h_3 \\
&\quad + 6K_{c2o}\cos(2\omega T_{2o})h_1h_3, \\
W_4 &= -6T_{2o}K_{c2o}^2h_3\sin(3\omega T_{2o})h_1 \\
&\quad - 4T_{2o}K_{c2o}\sin(\omega T_{2o})h_2^2 \\
&\quad - 6\sin(\omega T_{2o})T_{2o}K_{c2o}^2h_3h_1 \\
&\quad + 4\sin(3\omega T_{2o})T_{2o}K_{c2o}^2h_2^2 \\
&\quad - 4\sin(2\omega T_{2o})h_1h_2^2K_{c2o} \\
&\quad + 12\sin(2\omega T_{2o})h_1^2h_3K_{c2o}, \\
W_5 &= 24h_1h_3 - 8T_{2o}K_{c2o}\cos(\omega T_{2o})h_2^2h_1 - 12h_1^3h_3 \\
&\quad + 8h_2^2 - 8\cos(2\omega T_{2o})h_2^2K_{c2o} + 8h_1^2h_2^2 \\
&\quad - 12\cos(3\omega T_{2o})T_{2o}K_{c2o}^2h_3
\end{aligned}
$$

$$
\begin{aligned}
&- 24T_{2o}K_{c2o}\cos(\omega T_{2o})h_3 \\
&- 24\cos(2\omega T_{2o})h_3K_{c2o}h_1 \\
&+ 12T_{2o}K_{c2o}^2\cos(\omega T_{2o})h_3 \\
&+ 12T_{2o}K_{c2o}\cos(\omega T_{2o})h_1^2h_3,
\end{aligned}
$$

$$W_6 = 16T_{2o}K_{c2o}\sin(\omega T_{2o})h_2^2,$$

$$W_7 = -48h_1h_3 + 48T_{2o}K_{c2o}\cos(\omega T_{2o})h_3 + 32h_2^2,$$

$$
\begin{aligned}
D_0 = {} & h_1^2K_{c2o}^2 + 2K_{c2o}^2T_{2o}h_1\cos(3\omega T_{2o}) \\
&+ 2K_{c2o}^2T_{2o}\cos(\omega T_{2o})h_1 \\
&- 2K_{c2o}^3T_{2o}\cos(\omega T_{2o})h_1 \\
&+ K_{c2o}^4T_{2o}^2 + K_{c2o}^2T_{2o}^2 \\
&- 2K_{c2o}T_{2o}\cos(\omega T_{2o})h_1 \\
&- 2h_1^2K_{c2o}\cos(2\omega T_{2o}) \\
&- 2K_{c2o}^3T_{2o}^2\cos(2\omega T_{2o}) + h_1^2,
\end{aligned}
$$

$$
\begin{aligned}
D_1 = {} & 4K_{c2o}^2T_{2o}h_1^2\sin(\omega T_{2o}) \\
&- 4K_{c2o}^3T_{2o}^2h_1\sin(2\omega T_{2o}) \\
&+ 4K_{c2o}^2T_{2o}\sin(3\omega T_{2o}) - 4h_1^3K_{c2o}\sin(2\omega T_{2o}) \\
&+ 4K_{c2o}^2T_{2o}h_1^2\sin(3\omega T_{2o}) \\
&- 4K_{c2o}^2T_{2o}\sin(\omega T_{2o}) - 4K_{c2o}T_{2o}\sin(\omega T_{2o}) \\
&- 4K_{c2o}^3T_{2o}\sin(\omega T_{2o}),
\end{aligned}
$$

$$
\begin{aligned}
D_2 = {} & 4h_1^4 - 8K_{c2o}^2T_{2o}^2 + 4K_{c2o}^2 \\
&+ 8K_{c2o}^3T_{2o}^2\cos(2\omega T_{2o}) + 8K_{c2o}h_1^2\cos(2\omega T_{2o}) \\
&- 8K_{c2o}\cos(2\omega T_{2o}) - 8h_1^2 \\
&- 16h_1K_{c2o}^2T_{2o}\cos(3\omega T_{2o}) + 4K_{c2o}^2T_{2o}^2h_1^2 \\
&+ 16K_{c2o}T_{2o}\cos(\omega T_{2o})h_1 \\
&- 8K_{c2o}T_{2o}\cos(\omega T_{2o})h_1^3 + 4,
\end{aligned}
$$

$$
\begin{aligned}
D_3 = {} & -16K_{c2o}^2T_{2o}\sin(3\omega T_{2o}) - 16K_{c2o}h_1\sin(2\omega T_{2o}) \\
&+ 32K_{c2o}T_{2o}\sin(\omega T_{2o}) + 16K_{c2o}^2T_{2o}\sin(\omega T_{2o}) \\
&- 16K_{c2o}T_{2o}\sin(\omega T_{2o})h_1^2,
\end{aligned}
$$

$$
\begin{aligned}
D_4 = {} & 32h_1^2 + 16K_{c2o}^2T_{2o}^2 - 32 \\
&- 32K_{c2o}T_{2o}\cos(\omega T_{2o})h_1 \\
&+ 32K_{c2o}\cos(2\omega T_{2o}),
\end{aligned}
$$

$$D_5 = -64K_{c2o}T_{2o}\sin(\omega T_{2o}),\ D_6 = 64.$$

## References


1. Tondl, A.: Quenching of Self-excited Vibrations. Elsevier, Amsterdam (1991)
2. Sheng, G.: Friction-induced Vibrations and Sound: Principles and Applications. CRC Press, Boca Raton (2008)
3. Hinrichs, N., Oestreich, M., Popp, K.: On the modeling of friction oscillators. J. Sound Vib. **216**(3), 435–459 (1998)
4. Thomsen, J.J.: Using fast vibrations to quench friction-induced oscillations. J. Sound Vib. **228**(5), 1079–1102 (1999)
5. Panovko, Y.G., Gubanova, I.I.: Stability and Oscillations of Elastic Systems, Paradoxes, Fallacies and New Concepts. Consultants Bureau, New York (1965)
6. Ruina, A.: Slip instability and state variable friction laws. J. Geophys. Res. **88**(B12), 10359–10370 (1983)
7. McMillan, A.J.: A non-linear friction model for self-excited vibrations. J. Sound Vib. **205**(3), 323–335 (1997)
8. Canudas de Wit, C.C., Olsson, H., Astrom, K.J., Lischinsky, P.: A new model for control of systems with friction. IEEE Trans. Autom. Control **40**(3), 419–425 (1995)
9. Dupont, P., Hayward, V., Armstrong, B., Alpeter, F.: Single state elasto-plastic friction models. IEEE Trans. Autom. Control **47**(5), 787–792 (2002)
10. Swevers, J., Al-Bender, F., Ganseman, C., Prajogo, T.: An integrated friction model structure with improved presliding behavior for accurate friction compensation. IEEE Trans. Autom. Control **45**(4), 675–686 (2000)
11. Lampaert, V., Swevers, J., Al-Bender, F.: Modification of the Leuven integrated friction model structure. IEEE Trans. Autom. Control **47**(4), 683–687 (2002)
12. Lampaert, V., Al-Bender, F., Swevers, J.: A generalized Maxwell-Slip friction model appropriate for control purpose. In: Proceedings, IEEE International Conference, Physics and Control, vol. 4, pp. 1170–1177. St. Petersburg, Russia (2003)
13. Awrejcewicz, J., Olejnik, P.: Analysis of dynamic systems with various friction laws. Appl. Mech. Rev. **58**, 389–411 (2005)
14. Awrejcewicz, J., Olejnik, P.: Numerical and experimental investigations of simple non-linear system modeling a Girling duo-servo brake mechanism. In: ASME 2003 Design Engineering Technical Conferences and Computers and Information in Engineering Conference, Chicago, Illinois (2–6 September 2003)
15. Andreaus, U., Casini, P.: Dynamics of friction oscillators excited by a moving base and/or driving force. J. Sound Vib. **245**(4), 685–699 (2001)
16. Hetzler, H., Schwarzer, D., Seemann, W.: Analytical investigation of steady-state stability and Hopf-bifurcations occurring in sliding friction oscillators with application to low-frequency disc brake noise. Commun. Nonlinear Sci. Numer. Simul. **12**(1), 83–99 (2007)
17. Li, Y., Feng, Z.C.: Bifurcation and chaos in friction-induced vibration. Commun. Nonlinear Sci. Numer. Simul. **9**, 633–647 (2004)
18. Feeny, B.F., Moon, F.C.: Quenching stick–slip chaos with dither. J. Sound Vib. **237**(1), 173–180 (2000)
19. Popp, K., Rudolph, M.: Vibration control to avoid stick-slip motion. J. Vib. Control **10**(11), 1585–1600 (2004)

20. Chatterjee, S.: Non-linear control of friction-induced self-excited vibration. Int. J. Non-Linear Mech. **42**, 459–469 (2007)
21. Heckl, M.A., Abrahams, I.D.: Active control of friction driven oscillations. J. Sound Vib. **193**(1), 417–426 (1996)
22. Wagner, U., von, Hochlenert, D., Jearsiripongkul, T., Hagedorn, P.: Active control of brake squeal via 'smart pads'. SAE Technical Papers 2004-01-2773
23. Atay, F.M.: Van der Pol oscillator under delayed feedback. J. Sound Vib. **218**(2), 333–339 (1998)
24. Maccari, A.: Vibration control for the primary resonance of the van der Pol oscillator by a time delay state feedback. Int. J. Non-Linear Mech. **38**, 123–131 (2003)
25. Maccari, A.: The response of a parametrically excited van der Pol oscillator to a time delay state feedback. Nonlinear Dyn. **26**, 105–119 (2001)
26. Hu, H., Dowell, E.H., Virgin, L.N.: Resonances of a harmonically forced Duffing oscillator with time delay state feedback. Nonlinear Dyn. **15**, 311–327 (1998)
27. Masoud, Z.N., Nayfeh, A.H., Al-Mousa, A.: Delayed position-feedback for the reduction of payload pendulations of rotary cranes. J. Vib. Control **9**(1–2), 257–277 (2003)
28. Jnifene, A.: Active vibration control of flexible structures using delayed position feedback. Syst. Control Lett. **56**, 215–222 (2007)
29. Qian, C.Z., Tang, J.S.: A time delay control for a nonlinear dynamic beam under moving load. J. Sound Vib. **309**, 1–8 (2008)
30. Das, J., Mallik, A.K.: Control of friction driven oscillation by time-delayed state feedback. J. Sound Vib. **297**(3–5), 578–594 (2006)
31. Chatterjee, S.: Time-delayed feedback control of friction-induced instability. Int. J. Non-Linear Mech. **42**, 1127–1143 (2007)
32. Neubauer, M., Neuber, C., Popp, K.: Control of stick-slip vibrations. In: Proceedings of the IUTAM Symposium, Munich, Germany (18–22 July 2005)
33. Wahi, P., Chatterjee, A.: Averaging oscillations with small fractional damping and delayed terms. Nonlinear Dyn. **38**, 3–22 (2004)
34. Das, S.L., Chatterjee, A.: Multiple scales without center manifold reductions for delay differential equations near Hopf bifurcations. Nonlinear Dyn. **30**, 323–335 (2002)
35. Wahi, P., Chatterjee, A.: Regenerative tool chatter near a codimension 2 Hopf point using multiple scales. Nonlinear Dyn. **40**, 323–338 (2005)